Mar Biol (2008) 154:1–26
DOI 10.1007/s00227-007-0891-x

RESEARCH ARTICLE

# How do larvae attach to a solid in a laminar flow?

**G. Zilman · J. Novak · Y. Benayahu**

Received: 8 June 2007 / Accepted: 12 December 2007 / Published online: 5 February 2008


**Abstract** A hydrodynamic model explaining the mechanism of contact of marine larvae in vertical flows is presented. Two hydrodynamic factors—flow vorticity and larval self-propulsion—are the key components in the mathematical model. It is shown that flow vorticity causes a larva to rotate and change the direction of self-thrust, thus leading to its migration across the mean flow. The latter motion is of an oscillatory nature. Contact will be enabled only for sufficiently large amplitudes of oscillations. Simple expressions for the probability of initial contact are obtained for two-dimensional Couette and Poiseuille flows. The three-dimensional motion of a larva in a tube is studied using the Monte-Carlo simulations. It is shown that contact probability depends mainly on the ratio of the characteristic flow velocity and the larva's swimming speed. The theoretical results compare favorably with available experimental data. Possible applications of the method and results presented here to the classical problem of larval attachment to bodies of general geometry are briefly discussed in the concluding section.

**List of symbols**

| | |
|---|---|
| Bold letters | vector |
| Subscripts $X,Y,Z$ | projections of a vector on axes $O_1X$, $O_1Y$, $O_1Z$ |
| Subscripts $x,y,z$ | projections of a vector on axes $Ox$, $Oy$, $Oz$ |
| Subscript $O$ | denotes values calculated in the origin of the coordinate system $Oxyz$ |
| $a_{ik}$ | components of the matrix of cosines of directions |
| $\mathbf{b}(b_x, b_y, b_z)$ | radius vector of the center of buoyancy in the attached to the body coordinate system |
| $b_C = b_z$ | the distance between the center of gravity and the metacenter (metacentric height) |
| $B$ | volume of a body |
| $C$ | constant of integration |
| $d$ | distance between the wall and the center of mass of the larva |
| $D$ | diameter a of tube |
| $D_\mathrm{p}$ | diameter of a spherical body |
| $\mathbf{F}$ | total vector of hydrodynamic forces |
| $\mathbf{F}_\mathrm{B}$ | buoyancy force |
| $\mathbf{F}_\mathrm{D}$ | drag |
| $\mathbf{F}_\mathrm{T}$ | self-thrust |
| $\mathbf{g}$ | acceleration of gravity |
| $h$ | characteristic scale of a linear shear flow; width of the Couette channel; thickness of the linear boundary layer |
| $\mathbf{I}$ | tensor of mass moment of inertia |
| $\mathbf{j}_X$, $\mathbf{j}_Y$, $\mathbf{j}_Z$ | vector units of the axes of the inertial coordinate system |
| $L$ | characteristic length of the body |
| $m$ | the mass of a particle, larva |
| $\mathbf{M}$ | total vector of hydrodynamic moments |
| $\mathbf{M}_S$ | shear induced torque moment |
| $\mathbf{M}_B$ | hydrostatic moment |
| $O_1XYZ$ | right-hand orthogonal coordinate system fixed in space |

Communicated by S.W.A. Naqvi.

G. Zilman (✉) · J. Novak
Faculty of Engineering, School of Mechanical Engineering,
Tel Aviv University, 69978 Tel Aviv, Israel
e-mail: zilman@eng.tau.ac.il

Y. Benayahu
Faculty of Life Sciences, Department of Zoology,
Tel Aviv University, 69978 Tel Aviv, Israel

| | |
|---|---|
| $Ox'y'z'$ | moving coordinate system with axes parallel to those of $O_1XYZ$ |
| $Oxyz$ | right-hand orthogonal coordinate system fixed in a body |
| $P$ | probability of contact of a larva to a solid |
| $R$ | radius of a tube, half-width of a plane Poiseuille channel |
| $Re = U_\infty L/\nu$ | Reynolds numbers |
| $\mathbf{r}_O$ | radius-vector of the initial of the attached to the body coordinate system |
| Stk | Stokes number |
| $t$ | time |
| $t_p$ | particle relaxation time |
| $t_{contact}^{max}$ | maximal time which is necessary for a body to make contact |
| $\mathbf{U}$ | fluid velocity |
| $\mathbf{U}_O$ | fluid velocity calculated in the origin of the moving coordinate system |
| $\mathbf{U}_\infty$ | upstream velocity far from a body |
| $U_a$ | characteristic flow velocity |
| $\mathbf{V}$ | velocity of larva |
| $\mathbf{V}_S$ | larva's swimming velocity |
| $V_t$ | velocity of gravimetrical settlement |
| $\overline{V}_t = V_t/U_a$ | velocity of gravimetrical settlement scaled with the characteristic flow velocity |
| $X_O$, $Y_O$, $Z_O$ | coordinates of the initial of the fixed in the body coordinate system |
| $Z_O^0$ | coordinate of the center of mass of a body, larva at the initial moment of time |
| $\alpha$ | an angle designating the range $(-\alpha,\alpha)$ of initial angles of pitch of a larva |
| $\gamma_i$ | random number |
| $\delta$ | distance between the wall and the center of mass of the larva normalized with the tube diameter |
| $\Delta m$ | virtual mass of fluid |
| $\varepsilon$ | ratio of the buoyancy restoring moment and the shear stress torque moment |
| $\zeta$ | coordinate $Z_O$ normalized with the geometrical characteristic scale of a particular flow: $h$ for Couette or linear shear flows, $R$ for the Poiseuille channel or circular tube |
| $\zeta_0$ | coordinate $\zeta$ at the initial moment of time |
| $\theta$ | angle of roll |
| $\lambda$ | $= U_a/V_S$ |
| $\mu$ | fluid viscosity |
| $\nu$ | fluid kinematic viscosity |
| $\xi$ | longitudinal coordinate $X_O$ normalized with the geometrical characteristic scale of a particular flow: $h$ for Couette or linear shear flows, $R$ for the Poiseuille channel or circular tube |
| $\rho$ | fluid density |
| $\rho_p$ | mean density of a body |
| $\phi$ | angle of yaw |
| $\psi$ | angle of pitch |
| $\psi_0$ | initial angle of pitch |
| $\psi_e$ | $=\arcsin(1/\varepsilon)$-pitch angle providing stable motion of a larva without rotation |
| $\boldsymbol{\omega}$ | angular velocity of larva |
| $\boldsymbol{\Omega}$ | half of the vorticity vector, angular velocity of fluid particle |
| $\boldsymbol{\Omega}_O$ | half of the vorticity vector calculated in the origin of the moving coordinate system |

## Introduction

One or several consequent contacts of a larva with a rigid surface determine its future life stages, including attachment, settlement, metamorphosis and eventual survival. In 1991, Mullineaux and Butman formulated two questions of principal importance for larval ecology:

> *... Is initial contact of ... cyprids with a surface controlled by hydrodynamics, and does the probability of contact determine the cyprid's ultimate settlement site?*

Today it is well recognized that settlement of larvae on substrates is controlled not only by hydrodynamics but also by a large number of abiotic and biotic parameters (see e.g. Abelson and Denny 1997; Abelson et al. 1993, 1994; Eckman 1990; Eckman and Duggins 1998; Jonsson et al. 1991, 2004; Hart and Finelli 1999; Mullineaux and Butman 1990, 1991; Mullineaux and Garland 1993; Qian et al. 1999, 2000; Pasternak et al. 2004, Perkol-Finkel et al. 2006). However, as it was noted by Mullineaux and Garland (1993), the ability to distinguish between larval responses to flow from their responses to other surface cues, determines whether the effect of streams on larval contact is "... behavioral or purely hydrodynamic".

In this work, we are not intended to construct a mathematical model of contact mechanisms for all the infinite variety of larval forms and flow types. It is impossible. We consider here only certain hydrodynamics mechanisms of contact leaving apart numerous biotic and abiotic factors. Our study is restricted to simple but representative types of flows and larval forms. The technical task of our investigation is to calculate the contact probability for larvae moving in vortical flows and to compare it with experimental data. We thereby encounter a specific difficulty: for most of available experimental observations of larval behavior in well controlled flows the measured parameters are the settlement or the attachment rates, not the contact

rate. However, the contact probability $P$ and the settlement probability $P_{\text{settlement}}$ are not equal but related as:

$$P_{\text{settlement}} = PP_{\text{acceptance}}, \quad (1)$$

where the probability of acceptance $P_{\text{acceptance}}$ comprises behavioral responses of larvae to surface conditions or flow conditions and the history of the larvae (Mullineaux and Garland 1993). Many of marine species are able to undergo not one but several secondary settlements (e.g. Mullineaux and Butman 1991; Larsson and Jonsson 2006). In this respect, the probability of acceptance includes also the number of previous contacts. If settlement follows the first contact event, then the probability of contact and the probability of acceptance may be positively correlated but in any case the probability of initial contact of a larva with a substrate represents *an upper bound* of the attachment probability. Since it is difficult (if at all possible) to calculate the attachment probability, an estimate of its *upper bound* may be of great interest. This characteristic of the settlement phenomenon is studied theoretically in the present work.

The degree of complexity of hydrodynamic and mathematical models of larval motion depends on the complexity of the flows, in which the larvae move. Natural flows tend to be turbulent. The influence of turbulence on the settlement of marine larvae on different substrates is well recognized (see e.g. Crimaldi et al. 2002; Denny and Shibata 1989; Denny et al. 2002; Eckman 1990, 1996; Eckman and Duggins 1998; Jonsson et al. 2004; Mullineaux and Butman 1990, 1991).

In turbulent flows, fluid particles move unsteadily along complicated and unpredictable random trajectories, albeit in many turbulent processes the mean flow characteristics are not chaotic and can be described (at least in principle). Turbulent mixing may disperse marine larvae across the mean flow streamlines just as it disperses passive small particles. If the turbulence intensity is high then the role of turbulent mixing in delivering larvae to substrates is more important than the role of the mean transport; in other cases the situation can be the opposite. For instance, the bottom boundary layer created by not-steep waves can be laminar (e.g. Fredsøe and Deigaard 1992; Nilsen 1992). However, under steep and long waves, beneath breaking waves, along the sea shore, in rocky surf zones and on the rough bottom of a deep sea the corresponding boundary layers are turbulent. In turbulent boundary layers, turbulent mixing is the most probable mechanism for contact of propagules with substrata (Denny and Shibata 1989).

Contact due to turbulent mixing although it is an obviously important phenomenon, is however far beyond the scope of our study. We also do not consider such processes as those in which a larva may rapidly change the direction of motion due to strong pulsations in turbulent boundary layers.

Most of the analysis of the present work relates to laminar flows. Laminar fluid motions are observed in the sea bottom viscous sublayers, which thicknesses can vary within 0.5–6 mm (Archer 1989; Caldwell and Chriss 1979). If the size of a larva is much smaller then the depth of the viscous sublayer, and if the viscous sublayer is not affected strongly by turbulent pulsation then a mathematical model of larval motion in laminar flows can be used to explain larval contact with the sea bed. However, in many cases the viscous sublayer may be unsteady and only slightly thicker than the characteristic size of settling larvae.

Laminar boundary layers can be found on the upstream side of many bodies, or following the terminology by Abelson and Denny (1997) on the so-called protruding bodies. A broad class of such natural and artificial marine structures does exist in reality.

However, it is worth to consider first laminar flow in detail because that many of its features are presented in natural sea environment (Fredsøe and Deigaard 1992; Nilsen 1992) and because larval contact in laminar flows clues towards efficient methods of analyzing contact in natural flows. Contact phenomenon includes a huge number of biotic and abiotic factors which are mixed altogether. It may be hard to explain the overall cumulative effect of various factors influencing contact in turbulent flows without a clear understanding of the role and the relative importance of each of them in laminar flows.

In this work, we consider a principal contradiction of the contact phenomenon which only in laminar flows can be recognized in its pure essence. According to the modern paradigm of transport of passive larvae to substrates three different hydrodynamic mechanisms can be distinguished: the gravimetrical settling, transport by mean flow and turbulent mixing. Consider first such cases when larvae settling on substrates can not benefit from the gravitational sinking.

Qian et al. (1999) observed the attachment of *Bugula neritina* to clean walls of horizontal and vertical tubes when the flow inside the tubes was laminar or turbulent. It is not surprising that for turbulent flow regimes contact took place due to turbulent mixing. However, what can be the cause of larval contact in laminar flow?

For a fully developed laminar regime the fluid streamlines in a tube are parallel to the wall of the tube. Under such circumstances larvae making contact have to move in a direction perpendicular to the streamlines. For vertical tubes this effect can not be explained by the effective weight of a larva because it acts in the direction parallel to the tube's axis. Larvae of *B. neritina* are close to a sphere, their aspect ratio (the ratio of the length and beam) is about 1.1. Therefore, the hydrodynamic effect of non-sphericity on the dynamic of this larva may be considered as inessential in the first approximation (Swaminathan et al. 2006). Motion of *B. neritina* across the streamlines can not be explained by the hydrodynamic lift acting in the

direction perpendicular to the tube's axis because, in a laminar tube flow, small neutrally buoyant spherical particles concentrate at a distance of about 0.6 radii from the axis (Segre and Silberberg 1962). This distance is greater than the diameter of a particle by several orders of magnitude; whereas the distance that is required for a larva to initiate contact must be rather small, of an order of the characteristic length of a larva (Abelson and Denny 1997).

Larvae of *B. neritina* are phototactile (Lynch 1947) and may correct their position in response to light but in the paper by Qian et al. (1999) we did not find indications that motion of larvae was affected by the overall illuminations of the tubes or by contrasts of the light and shadow. Therefore, we infer that the only cause of larval motion across the main stream is their motility. Do larvae choose this direction of motion deliberately, is the motions across the streamlines imposed by hydrodynamics solely, or is the transverse drift a result of a combination of behavioral and hydrodynamic factors? In this respect, it is interesting to quote Lynch (1947):

> *The larvae of B. neritina, however, under ordinary laboratory conditions ... were never observed to become negatively phototactic at any time; swarms of metamorphosed larvae could always be found on the lighted side of the container within an hour after they had been shed. Furthermore, they maintained a definitely negative geotaxis throughout the entire larval period and attached to the sides of the container, but fixation always took place at or near the surface. Here, then, was a paradox! What factors in nature, not operative under the unusual conditions of the laboratory, could be responsible for causing larvae to attach near the bottom of the channel and in regions not exposed to the direct light of the sun?*

In the present work, we are seeking the answer to the above question in the hydrodynamics of a larva which is different in sea currents and in a still water of a laboratory tank, the fact revealed first by Butman et al. (1988).

Larvae settle on a vertical protruding body, e.g., on vertical cylinders (Abelson and Denny 1997). Whether the flow regime around such a body is turbulent or laminar is determined by the corresponding Reynolds number $Re = U_\infty L/\nu$, where $U_\infty$ is the ambient mean fluid velocity, $L$ is the characteristic diameter of the cylinder and $\nu$ is the kinematic viscosity of the fluid. If the Reynolds number exceeds a certain threshold $Re > 5 \times 10^5$, it is common to say that the fluid motion around the cylinder is turbulent. A silent feature of such a "turbulent" flow is that on the front upstream part of the cylinder the fluid motion can be considered as laminar (Achenbach 1968; Schlichting 1979; Roshko 1961; Scorer 1978). The extent of the laminar zone depends on the Reynolds number but, roughly speaking, the boundary layer on the entire front (upstream) part of the cylinder is laminar.

A small rigid particle approaching a large body moves very approximately along the fluid streamlines, which do not cross the body surface. However, the most inertial particles may deviate from the streamlines and hit the obstacle (Scorer 1978). The probability of contact of a passive larva with an obstacle is strongly related to the efficiency of catch of a cloud of rigid particles by a large body. In the theory of aerosols and hydrosols, the efficiency of catch is defined as the proportion of the particles lying in the cylinder swept out by the geometrical outline of the body which actually collide with and are captured by that body (Scorer 1978). As it follows from the theory of aerosols and hydrosols, the probability of contact of a small rigid particle of diameter $D_p$ with a large cylinder of diameter $L$ ($L \gg D_p$) is determined by the Stokes' number,

$$\mathrm{Stk} = \left(1 + \frac{\rho}{2\rho_p}\right)\frac{\rho_p U_\infty D_p^2}{18\mu L}, \qquad (2)$$

where $\rho$ is the density of water, $\rho_p$ is the mean density of the rigid particle, and $\mu$ is the water viscosity (Fuchs 1964; Seinfeld and Pandis 1998). For a larva of diameter of 200 μm and for an obstacle of 1 cm length the Stokes' number is small to such and extent that the efficiency of catch is practically zero (Fuchs 1964). However, larvae do settle in a horizontal stream on a vertical body of a diameter, which can be much larger than 1 cm.

It is even more surprising that larvae settle on bodies of small cross-section areas, e.g. on relatively thin plates which are aligned with the mean stream and where the gravimetrical settlement also does not influence contact significantly (Mullineaux and Butman 1991; Mullinaux and Garland 1993). Mullineaux and Butman (1991) considered larval settlement on three types of plates: a thin plate with a sharp edge, a somewhat thicker plate with rounded ends, and a combination of two perpendicular plates (Fig. 1). Mullineaux and Butman (1991) explain larval contact in these experiments by the flow advection towards the plates in the area of the reattachment of the flow, which has been separated at the leading edges of the plates. However, it can be seen from Fig. 1a that for a thin plate the mean flow is directed away from it. It is unlikely that in this particular case contact is caused by turbulent mixing. In this respect, Mullineaux and Butman (1991) on p. 98, and p. 102 of their work made several important remarks:

> *Cyprid contact was significantly correlated with the vertical advection on the most of the plates, but was not consistently related to either turbulence or shear stress ... Turbulence ... seems to play lesser role in initial contact.*

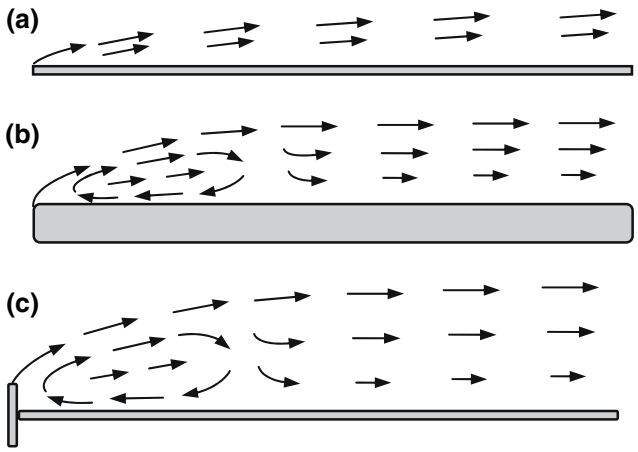


**Fig. 1** Schematic drawing of the experimental results of Mullineaux and Butman (1991) with mean streamlines for three types of plates. The mean flow is directed away from the thin plate (**a**). On a thick (**b**) and split (**c**) plates flows in the vicinity of their leading edges are characterized by large vortices that may be responsible for larval transport toward the plates. One of the causes of larval transport to the plate (**a**) may be turbulent mixing. However, it is also possible that contact is due to the mean vorticity, which rotates a larva and alters the direction of its self-thrust

This quotation should be understood in the context of the problem considered, i.e., that the particular values of the turbulent intensity in this particular experiment do not influence drastically the contact phenomenon. Nevertheless, how do passive larvae make contact if the mean streamlines of the flow do not cross the surface, the mean advection is away from the surface, and turbulence mixing is not a significant factor influencing contact?

Finally, if the concept of a passive transport of larvae to substrate cannot consistently explain many cases of larval contact, we return to the same question by Mullineaux and Butman (1991) which is reformulated here as follows: "How do larvae attach to a bounding surface, *when contact is seemingly highly improbable*?"

In attempting to answer this long-standing question, we studied here the mechanisms of larval contact in a linear shear flow, in a plane channel and in a tube. We chose to study larval contact in linear shear and Poiseuille flows not only because of their relative simplicity but also because they have many important similarities with a laminar part of a boundary layer of a body with a laminar or turbulent wake. The linear shear flow approximation may be used to explain the properties of a boundary layer with a more complex velocity profile (Schlichting 1979) or can be applied to explain the motion of living organisms even in a turbulent environment (see e.g. Karp-Boss and Jumars 1998; Grünbaum and Strathnman 2003).

We consider examples of flow which are vortical. All real flows, laminar or turbulent, are vortical. The flow vorticity can be imagined as twice angular velocity $\boldsymbol{\omega}$ of a small volume of fluid translating with the velocity fluid vector $\mathbf{U}$. The relation between the flow vorticity and the angular velocity $\boldsymbol{\Omega}$ is expressed as

$$\boldsymbol{\Omega} = \frac{1}{2}\operatorname{curl}\mathbf{U}, \tag{3}$$

where the mathematical operation curl $\mathbf{U}$ is explained in Appendix IV. A small rigid spherical particle in viscous non-uniform flow also rotates due to the shear stresses on its surface, and its angular velocity $\boldsymbol{\omega}$ is close to the angular velocity $\boldsymbol{\Omega}$ of a small volume of fluid, i.e.,

$$\boldsymbol{\omega} \approx \boldsymbol{\Omega}. \tag{4}$$

In 1955, Crisp noted that in a laminar tube flow larvae rotate. They behave passively and do not use their self-thrust if the shear rate calculated on the wall of the tube is relatively low. However, when the wall shear rate exceeds a certain limit (different for different species), cyprids start to behave actively: they use their locomotion devices, develop a certain swimming speed and, as a result, attach to the wall.

> It was interesting to note that at lower rates of flow the cyprids often did not swim, but were rolled passively ... by the current. This passive behavior was progressively less in evidence as the rate of shear increased, and the highest percentage of attachment in *B. balanoides* occurred between 60 and 80 $s^{-1}$. When the rate of shear exceeded 50 $s^{-1}$ the cyprids were stimulated to great swimming activity and often attached immediately. (Crisp 1955).

The above quotation refers to species of *Balanus balanoides*, but for the estuary specie *Eliminus modestus* the situation is similar, except that maximum attachment was achieved at the threshold values of the shear rate—about 45–50 $s^{-1}$.

In fact, in each point of a tube the shear rate (the velocity gradient in the radial direction) also represents the fluid vorticity. Bearing this in mind, we are now ready to formulate the central biological assumption of our work, which couples the hydrodynamic and biological factors.

Based on observations of Crisp (1955), we assume that it is the larva's rotation in vortical flows that triggers the mechanism of self-propulsion, i.e., a rotating larva develops self-thrust (Fig. 2). In a tube the shear rate is maximal on the wall; on the axis of the tube it is zero. It follows from the experiments of Crisp (1955) and Qian et al. (1999) that the probability of larval attachment in laminar flows may be rather high and it is unlikely that only larvae that enter a tube close to the wall can make contact. It is more probable that larvae start to swim at such values of

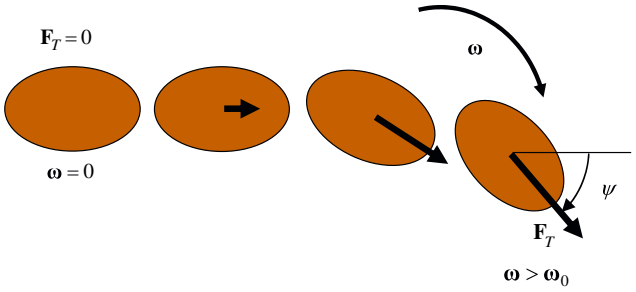


**Fig. 2** A larva entering a shear flow and moving from left to right with the main stream. In the initial left position of the larva the flow is irrotational, the larva does not rotate and does not use thrust $\mathbf{F}_T$. In a shear flow the larva starts to rotate due to the flow vorticity with an angular velocity $\omega$. If the angular velocity $\omega$ exceeds a certain threshold $\omega_0$, the larva develops self-thrust. Due to the rotation of the vector of the self-thrust the larva changes the direction of motion. It is characterized by an angle $\psi$, which is measured with respect to the direction of the mean flow. Due the rotation of the vector of the self-thrust the larva migrates across the mean flow

the flow vorticity, which are much smaller than those on the wall. The corresponding threshold values of the vorticity and of the angular velocity of a larva may be species specific, and they are not known exactly. Under such circumstances we assume that a larva starts to swim at even a very small value of the flow vorticity by developing the maximal available thrust, which remains constant in the process of motion.

## Methods

### Assumptions

We refer to a larva with a body that can be considered as a rigid particle. We assume that the larva is small, i.e., that its typical length is much smaller than the characteristic scale of the spatial flow variations. In tubes or channels this scale is of the same order of magnitude as the diameter of the tube or the width of the channel. For outer flows the scale relates to the thickness of the boundary layer of the body catching the larva.

Strictly speaking, our formulation pertains to laminar regimes of fluid motion. However, it is important to note that it comprises the mechanism of larval contact with bodies which may have a fully turbulent wake but a laminar boundary layer on their upstream part.

In some parts of our analysis in order to obtain analytic results we shall assume that physical contact of a larva with a substrate occurs when the larva's center of mass reaches the rigid surface. In other words, a larva is considered as a point that behaves in a flow as a particle of finite albeit small diameter, a restriction which is lifted further in the numerical simulations.

We consider larval contact only in slowly varying flows. Correspondingly, it is also assumed that a larva moves slowly with respect to the ambient flow and that the hydrodynamic forces acting on it can be described within the framework of the low Reynolds number hydrodynamics (Happel and Brenner 1983). Whether the flow varies "slowly" or "fast" can be estimated by evaluating the relaxation time of larval motion

$$t_{\mathrm{p}} = \frac{m + \Delta m}{3\pi\mu D_{\mathrm{p}}}, \tag{5}$$

where $m$ is the mass of the particle (Seinfeld and Pandis 1998) and $\Delta m$ is the added mass of the fluid (Lamb 1945). Relaxation time is the time for which a passive particle starting its motion with zero velocity in a steady flow reaches 63% of the flow velocity. For instance, for a larva of an equivalent diameter of an order of 250 μm the viscous relaxation time is of order of 5 ms. For most larva of interest the relaxation time is very short comparing to the typical characteristic time of the entire process under consideration, the time which is needed for a larva to reach the substrate. We consider such larvae as inertialess.

Many marine larvae, by progressing forward in still water or a uniform flow rotate about their anterior–posterior axis and move along a helix-like path (Jonsson et al. 1991; Maldonado 2006; Pasternak et al. 2004; Wendt 2000). There is experimental evidence that the radius of the corresponding helix is of the same order of magnitude as the larva's characteristic length (Jonsson et al. 1991) and, thus, is small compared to the characteristic length of the spatial flow variations. Correspondingly, in the subsequent kinematic analysis such small trajectory variations are disregarded.

Many larvae have a quite complex morphology which may influence their hydrodynamics and the kinematics of motion, including the angular velocity of their rotation in shear flows (Karp-Boss and Jumars 1998; Karp-Boss and Boss 2000). Since the angular velocity influences larval trajectories and the trajectories determine the contact probability, the later is a function of the shape of a larva. Because of the huge variety of larval forms it is extremely difficult to deal with their true geometry. An alternative way to tackle the problem is to present the larva's body as an equivalent rigid spherical or an ellipsoidal particle with the same mass and volume as those of the larva.

In a linear shear flow, a neutrally buoyant inertialess spherical particle moves along streamlines and rotates with constant angular velocity, whereas an elliptical particle has a preferable direction aligned with the flow and rotates with an angular velocity according to the orbits of Jeffery (1922). However, for an inertialess ellipsoid with negative buoyancy moving in a vertical tube the results may be different (Swaminathan et al. 2006; Sugihara-Seki 1996).

Swaminathan et al. (2006) studied theoretically the motion of an inertialess negatively buoyant rigid ellipsoidal particle settling in a laminar flow of a circular tube and found, that under Stokes flow conditions, an ellipsoid without inertia is observed to follow a perfectly periodic helical orbit in which it rotates, moves along the tube and across the stream lines. The amplitudes and periods of this oscillatory motion depend on the initial orientation and the aspect ratio of the ellipsoid. For instance, if an ellipsoid with the ratio of its length and maximal beam equal to 2 enters a tube with an initial angle of 15° with respect to the tube's axis then the amplitude of oscillations of the ellipsoid across the mean flow is about 0.15 of the tube radii. If the entrance angle is about 65°, then the amplitude of oscillations is about 0.75 of the tube radii. From the numerical simulations of Swaminathan et al. (2006), we infer that a slender ellipsoid without self-propulsion moving in a relatively narrow tube does not make contact with the wall unless its entrance angle approaches to 90°. It is rather unlikely that all larvae enter a tube with the same 90° angle.

It should be noted also that calculations by Swaminathan et al. (2006) pertain to a tube with a radius only four times larger than the longitudinal semi-axis of the ellipsoid. We consider tubes of diameters by order of magnitudes larger than the diameter of larvae moving in these tubes and larvae with an aspect ratio less than two.

The discussed above features of motion of a slender particle in a vortical flow take into account its effective weight, which can be considered as a thrust always acting in the same direction. If a rigid particle is swimming due to self-thrust, which can change direction, its trajectory too may be affected by this factor (Pedley and Kessler 1992). It is possible that the rotating vector of the thrust is a more potent contributor to the particle drift across the mean flow than the slenderness of the body. Correspondingly, in this work we consider larvae with a small degree of non-sphericity but motile, not passive. The shape of a larva is characterized here by the only parameter, its equivalent diameter $D_p$.

Once we consider a spherical larva, its center of buoyancy and center of hydrodynamic forces are located in the center of the sphere. However, due to the non-uniform density of many larvae their center of gravity may not coincide with the center of buoyancy. If all hydrodynamic and hydrostatic moments acting on a larva are calculated about the origin of the coordinate system located in the center of gravity, then rotation of a larva leads to a hydrostatic buoyancy moment. This moment may influence a larva's equilibrium position, its angular velocity and the direction of motion (see e.g. Kessler 1986). Therefore, the general formulation of the problem under consideration includes the hydrostatic force and moment.

To calculate the hydrodynamic forces acting on a larva we use the hydrodynamic theory of low Reynolds numbers. We consider a larva as a smooth rigid (non-deformable) body with a non-slip condition on its surface. Real larvae, however, are neither smooth nor rigid. In the course of their motion larvae can change their shape and volume. In our investigation, however, we do not take all these factors into account and consider only the first approximation of the form of a lava: a rigid smooth sphere.

## Coordinate systems

Three right-hand orthogonal coordinate systems are used here: fixed in space $O_1XYZ$, fixed in the body of a larva-particle $Oxyz$, and an auxiliary coordinate system $Ox'y'z'$, which moves with the larva-particle while its axes remain parallel to the axes of the fixed in the space coordinate system (Fig. 3). The orientation of the axes of the attached to the body coordinate system is determined by three Euler angles and the corresponding matrix of the cosines of directions (Fig. 3).

The motion of a larva-particle can be represented as a translation described in the fixed in space coordinate system $O_1XYZ$ by the vector of linear velocity $\mathbf{V}(V_X, V_Y, V_Z)$ of the origin $O$ and the rotation with the angular velocity $\boldsymbol{\omega}(\omega_x, \omega_y, \omega_z)$. The origin of the moving coordinate systems in the inertial coordinate system is determined by its radius vector $\mathbf{r}_O$ $(X_O, Y_O, Z_O)$ and its velocity can be calculated as the derivative of the radius vector with respect to time $t$

$$\frac{\mathrm{d}\mathbf{r}_O}{\mathrm{d}t} = \mathbf{V}. \tag{6}$$

The relations between the Euler angles and the corresponding components of the angular velocity $\boldsymbol{\omega}(\omega_x, \omega_y, \omega_z)$ on the axes of the fixed in the body coordinate system are given as follows (Goldstein et al. 2002):

$$\begin{aligned} \frac{\mathrm{d}\phi}{\mathrm{d}t} &= (\omega_z \cos\theta + \omega_y \sin\theta)\sec\psi, \\ \frac{\mathrm{d}\psi}{\mathrm{d}t} &= \omega_y \cos\theta - \omega_z \sin\theta, \\ \frac{\mathrm{d}\theta}{\mathrm{d}t} &= \omega_x + (\omega_z \cos\theta + \omega_y \sin\theta)\tan\psi. \end{aligned} \tag{7}$$

The radius vector $\mathbf{r}_O$ and the angular velocity $\boldsymbol{\omega}$ determine the location of a larva and its orientation in space.

For an arbitrary vector $\mathbf{A}$, its components in the coordinate systems $O_1XYZ$ and $Oxyz$ are related as follows:

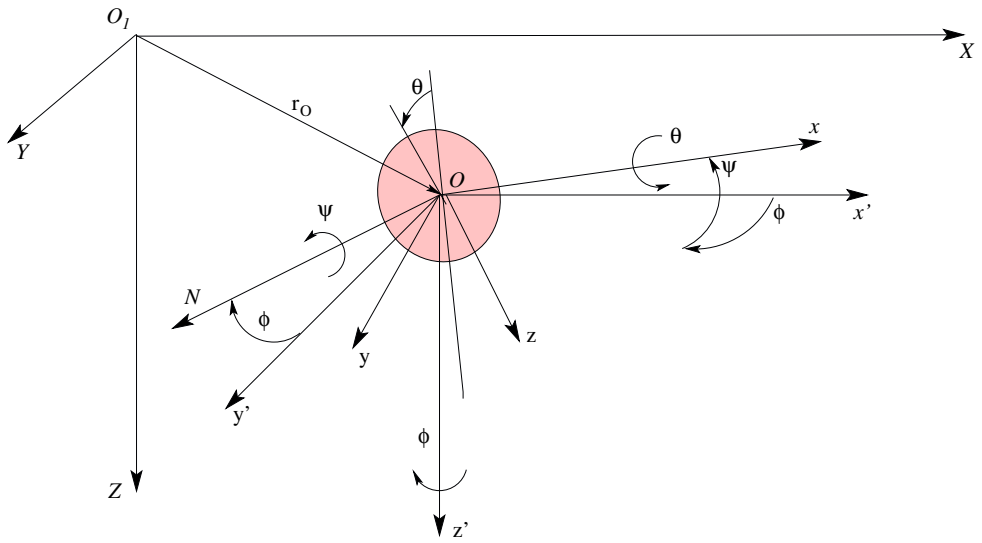


**Fig. 3** Orthogonal right-hand coordinate systems: fixed in space $O_1XYZ$ and fixed in the body $Oxyz$. The origins of the moving coordinate systems coincide with the center of mass of the larva-particle. The unit vectors of the fixed in the space coordinate system are denoted as $\mathbf{j}_X$, $\mathbf{j}_Y$ and $\mathbf{j}_Z$, respectively. The rotation of the fixed in the body coordinate system $Oxyz$ as a whole is described by three Euler's angles ($\phi$, $\psi$, $\theta$), which can be chosen in different ways. We chose here a coordinate system with the line of nodes defined as the line of intersection of the planes $x'Oy'$ and $yOz$. The angle of yaw $\phi$ represents the rotation around $Oz'$ axis, the rotation about the line of nodes is described by the angle pitch $\psi$, and the angle of roll $\theta$ corresponds to the rotation around the $Ox$ axis. The relation between the coordinate systems $Ox'y'z'$ and $Oxyz$ is given by the following transformation matrix of the cosines of the directions $\begin{array}{c|ccc} & x & y & z \\ x' & a_{11} & a_{12} & a_{13} \\ y' & a_{21} & a_{22} & a_{23} \\ z' & a_{31} & a_{32} & a_{33} \end{array}$ where the elements of the matrix $a_{ik}$ ($i,k$ = 1,2,3) are given as follows: $\begin{array}{lll} a_{11} = \cos\phi\cos\psi, & a_{21} = \sin\phi\cos\psi, & a_{31} = -\sin\psi \\ a_{12} = \sin\theta\cos\phi\sin\psi - \cos\theta\sin\phi, & a_{22} = \cos\theta\cos\phi + \sin\theta\sin\phi\sin\psi, & a_{32} = \sin\theta\cos\psi \\ a_{13} = \cos\theta\cos\phi\sin\psi + \sin\theta\cos\phi, & a_{23} = \cos\theta\sin\phi\sin\psi - \sin\theta\cos\phi, & a_{33} = \cos\theta\cos\psi \end{array}$ It should be noted that the direction of the axis $O_1Z$ in the figure does not relate to any preferable direction in space. If the gravity and buoyancy effects are essential then vector of acceleration of gravity is directed in the negative direction of the axis $O_1Z$, i.e., $\mathbf{g} = -g\mathbf{j}_Z$, where $g$ = 9.81 m/s$^2$. The vector of buoyancy force is pointing in the positive direction of the axis $O_1Z$. However, if we consider motion of a larva in a linear shear flow created by two vertical walls (Couette channel) or a linear shear flow in a physical horizontal plane then the axis $O_1Z$ is directed perpendicularly to the walls of the channel then the gravity and buoyancy forces are not involved in the analysis

$$A_{x_k} = \sum_{k=1}^{3} a_{ik}A_{X_i},\ A_{X_k} = \sum_{k=1}^{3} a_{ki}A_{x_i}, \tag{8}$$

where $x_1 \equiv x$, $x_2 \equiv y$, $x_3 = z$ and $X_1 \equiv X$, $X_2 \equiv Y$, $X_3 \equiv Z$. For instance, if $\mathbf{A}$ is a vector of self-thrust $F_T$ acting in a posterior–anterior direction it can be assumed that in the attached to the body coordinate system its components are ($F_T$, 0,0). In such a case the components of the same vector in the inertial coordinate system can be expressed as follows:

$$F_{TX} = a_{11}F_T,\ F_{TY} = a_{21}F_T \text{ and } F_{TZ} = a_{31}F_T. \tag{9}$$

For a two-dimensional motion in the plane $O_1XZ$ relations 9 will be as the follows:

$$F_{TX} = F_T\cos\psi \text{ and } F_{TZ} = -F_T\sin\psi. \tag{10}$$

Equation 10 is used in the sequel to analyze the motion of a larva in two-dimensional plane flows.

## Equations of motion

In the fixed in-space inertial coordinate system the motion of a sphere moving with linear velocity $\mathbf{V}$ under the action of body and surface forces $\Sigma\mathbf{F}$ is described by the equation of conservation of momentum:

$$(m + \Delta m)\frac{d\mathbf{V}}{dt} = \Sigma\mathbf{F}(t), \tag{11}$$

where $m = B\rho_p$, $B$ is the volume of the body, $\rho_p$ is the average density of the body, $\Delta m = \rho Bk$ and $k$ is the added mass coefficient depending on the form of the body and equal 1/2 for a sphere (Lamb 1945).

The rotation of the body is described in the fixed in the body coordinate system by the equation of conservation of the angular momentum:

$$\mathbf{I}\frac{d\boldsymbol{\omega}}{dt} + \boldsymbol{\omega}\times(\mathbf{I}\boldsymbol{\omega}) = \Sigma\mathbf{M}(t), \tag{12}$$

where $\mathbf{I}$ is the mass moment inertia tensor and $\sum\mathbf{M}$ is the total torque moment.

The reaction acting on the body can be represented as a sum of gravity, buoyancy, surface and self-propulsion forces and moments:

$$\sum \mathbf{F}(t) = \mathbf{F}_{\mathrm{G}} + \mathbf{F}_{\mathrm{B}} + \mathbf{F}_{\mathrm{D}} + \mathbf{F}_{\mathrm{T}}, \tag{13}$$

$$\sum \mathbf{M}(t) = \mathbf{M}_{\mathrm{G}} + \mathbf{M}_{\mathrm{B}} + \mathbf{M}_{\mathrm{D}} + \mathbf{M}_{\mathrm{T}} + \mathbf{M}_{\mathrm{S}}, \tag{14}$$

where subscripts G, B, D, T and S correspond to the gravity, buoyancy, drag, thrust and surface forces and moments.

The gravity $\mathbf{F}_{\mathrm{G}}$ and buoyancy forces $\mathbf{F}_{\mathrm{B}}$ are given as follows:

$$\mathbf{F}_{\mathrm{G}} = \rho_p B\mathbf{g}, \tag{15}$$

$$\mathbf{F}_{\mathrm{B}} = -\rho B\mathbf{g}, \tag{16}$$

where $\mathbf{g}$ is the acceleration of gravity. The total vector of these body forces is the effective weight given by the following relation:

$$\mathbf{F}_{\mathrm{GE}} = (\rho_p - \rho)B\mathbf{g}, \tag{17}$$

where for a larva with negative buoyancy

$$\rho_p - \rho > 0. \tag{18}$$

Since the center of the attached to the body coordinate system is placed in the center of gravity then $\mathbf{M}_{\mathrm{G}} = 0$; whereas the buoyancy force gives the following moment of a hydrostatic nature:

$$\mathbf{M}_{\mathrm{B}} = \rho(\mathbf{b} \times \mathbf{g})B, \tag{19}$$

where $\mathbf{b}(b_x, b_y, b_z)$ is the radius-vector of the center of buoyancy in the fixed in the body coordinate system (Fig. 4).

Equations 15–19 incorporate the vector of the acceleration of gravity. Its projection on the axis of the fixed in the space coordinate system $O_1Z$ is $g_Z = -g$; whereas the corresponding projections on the axes of the fixed in the body coordinate system are given by 8. If we consider larvae making contact with a horizontal substrate then the effective weight and the buoyancy moment have to be included into the analysis. For a larva making contact with a vertical substrate the gravitational and buoyancy forces can be neglected.

We assume that in the attached to the body coordinate system the coordinates of the center of buoyancy are given by $b_x = b_y = 0$ and $b_z = b_C$, where $b_C$ is a positive quantity representing the metacentric height. Such a configuration provides the stability of the equilibrium position of a larva and does not restrict the generality of the consequent analysis.

The surface hydrodynamics reactions are due to the normal and shear stresses applied to the surface of the body and resulting in the drag $\mathbf{F}_{\mathrm{D}}$ and the torque moment $\mathbf{M}_{\mathrm{S}}$. For a sphere moving with low Reynolds numbers they can be evaluated within the framework of the low Reynolds number hydrodynamics as follows (Happel and Brenner 1983):

$$\mathbf{F}_{\mathrm{D}} = -3\pi\mu D_{\mathrm{P}}(\mathbf{V} - \mathbf{U}_O), \tag{20}$$

$$\mathbf{M}_{\mathrm{S}} = \pi\mu D_{\mathrm{p}}^3(\mathbf{\Omega}_O - \boldsymbol{\omega}), \tag{21}$$

where $\mathbf{U}_O$ and $\mathbf{\Omega}_O$ are the fluid velocity and the half of the vorticity vector calculated in the center of the sphere.

The value of the vector of the self-propulsion force $\mathbf{F}_{\mathrm{T}}$ can be estimated by noting that during steady motion in still water the drag of a larva and its self-thrust are equal by their absolute values and are directed oppositely. Correspondingly, the Stokes' formula 20 gives the value of the self-thrust as a linear function of the larva's swimming velocity $\mathbf{V}_{\mathrm{S}}$:

$$\mathbf{F}_T = 3\pi\mu D_p\mathbf{V}_{\mathrm{S}}.$$

For a larva of spherical form the drag and the thrust create a corresponding moment about the center of gravity, as is shown in Fig. 4.

For an inertialess particle the left-hand sides in Eqs. 11–12 can be disregarded yielding equations of quasi-static equilibrium

$$\sum \mathbf{F}(t) = 0 \tag{22}$$

and

$$\sum \mathbf{M}(t) = 0. \tag{23}$$

In such a quasi-steady motion the sum of the drag and of the self-propulsion vector is equal to zero and therefore the total hydrodynamic moment which is created by these two forces is also equal to zero (Fig. 4).

Dividing all terms of Eq. 22 by $3\pi\mu D_{\mathrm{P}}$, all terms of Eq. 23 by $\pi\mu D^3{}_{\mathrm{p}}$ and recalling that the volume of the body is given by $B = \pi D^3{}_{\mathrm{p}}/6$, the equations of balance of all hydrodynamic forces and moments result in the following relations:

$$\mathbf{V} = \mathbf{U}_O + \mathbf{V}_{\mathrm{S}} + \mathbf{V}_t, \tag{24}$$

$$\boldsymbol{\omega} = \mathbf{\Omega}_O + \boldsymbol{\omega}_b, \tag{25}$$

where

$$\mathbf{V}_t = \frac{(\rho_p/\rho - 1)D_{\mathrm{p}}^2}{18\nu}\mathbf{g} \tag{26}$$

is the velocity of gravitational settlement of the body and

$$\boldsymbol{\omega}_b = \frac{\mathbf{b} \times \mathbf{g}}{6\nu} \tag{27}$$

is the angular velocity of the body induced by the hydrostatic buoyancy moment which depends on three Euler angles (see e.g. Fig. 4 for a two-dimensional case). In the state of an

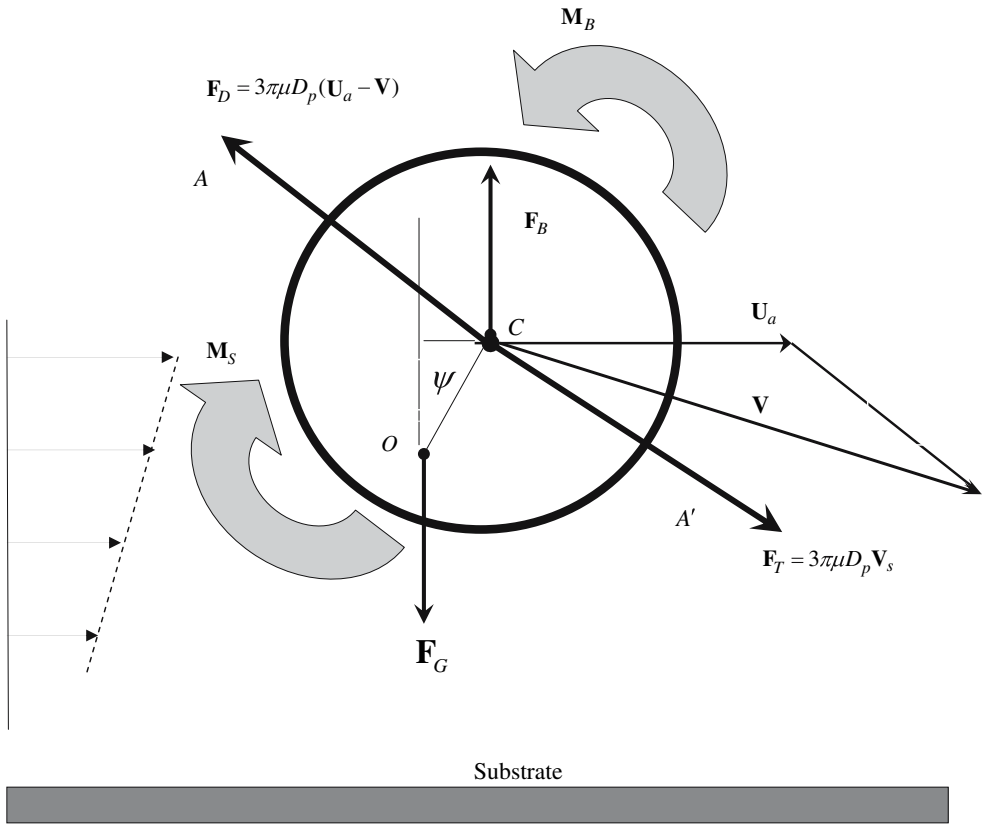


**Fig. 4** Forces and moments acting on a body with an axis of symmetry $AA'$, which passes through the centroid of the body. In steady or slow motion the sum of the surface hydrodynamic force $\mathbf{F}_D$ and of the self-propulsion force is zero. The body moves with the velocity $\mathbf{V}$, which represents a geometrical sum of the swimming velocity $\mathbf{V}_S$ and the fluid velocity $\mathbf{U}_a$, calculated in the centroid $C$. The center of gravity and buoyancy do not coincide. The buoyancy moment calculated about the center of gravity is $M_B = F_B\left|\overrightarrow{OC}\right|\sin\psi$, where $\overrightarrow{OC} = \mathbf{b}$ is the radius vector of the center of buoyancy $C$ in the fixed to the body coordinate system. For a fully submerged body $C$ is the so-called metacenter and the distance $OC$ is the metacentric height (terminology, which was introduced by Euler in his classical work on the theory of ships). For a body with a posterior-anterior axis of symmetry the surface force $\mathbf{F}_D$ acts along the axis $AA'$. If the vector of the self-propulsion force also acts along the same axis then the total moment of the both reactions about any point is obviously zero. Due to the shear stress torque moment $\mathbf{M}_S$ the body rotates in the clockwise direction, whereas the buoyancy moment $\mathbf{M}_B$ acts in the counter-clock direction. If the magnitudes of the moments are equal, then the body approaches the substrate without rotation. If the shear induced torque moment exceeds the maximal value of buoyancy moment then the body and the vector of the self-thrust $\mathbf{F}_T$ also rotate

equilibrium larva does not rotate and three Euler angles can be found from the three scalar equations following from one vector Eq. 25 when its left-hand side is zero:

$$\mathbf{\Omega}_O + \boldsymbol{\omega}_b = 0. \tag{28}$$

The linear and angular velocities, Eq. 24, 25, can be substituted into the right-hand side of Eqs. 6 and 7, yielding a system of six ordinary differential equations with respect to three coordinates of the center of mass of the larva and three Euler angles.

## Equations of larval motion in two-dimensional linear shear and Poiseuille flows

Consider the motion of a larva in the plane $O_1XZ$. For such two-dimensional flow the vector of translational velocity has two non-zero components $V_X$ and $V_Y$ whereas the vector of angular velocity $\boldsymbol{\omega}$ has only one component $\omega_y \equiv \omega$. The fluid velocity vector $\mathbf{U}$ is directed along the longitudinal axis and varies linearly with the coordinate $Z$:

$$\mathbf{U} = 2U_a\frac{Z}{h}\mathbf{j}_X. \tag{29}$$

Here $h$ is the distance above the bottom where the fluid velocity reaches the value $2U_a$ (Fig. 5). Relation 29 can be interpreted in several ways. It can represent a flow unbounded from above (linear shear flow), a flow where the fluid velocity varies linearly within a layer of depth $h$ and is constant and equal to $2U_a$ outside the layer (linear boundary layer, Schlichting 1979) and a flow between two plates, where one of them is fixed and the other one moves with velocity $2U_a$ (Couette flow). In all three cases the characteristic geometric scale of the flow $h$ and the

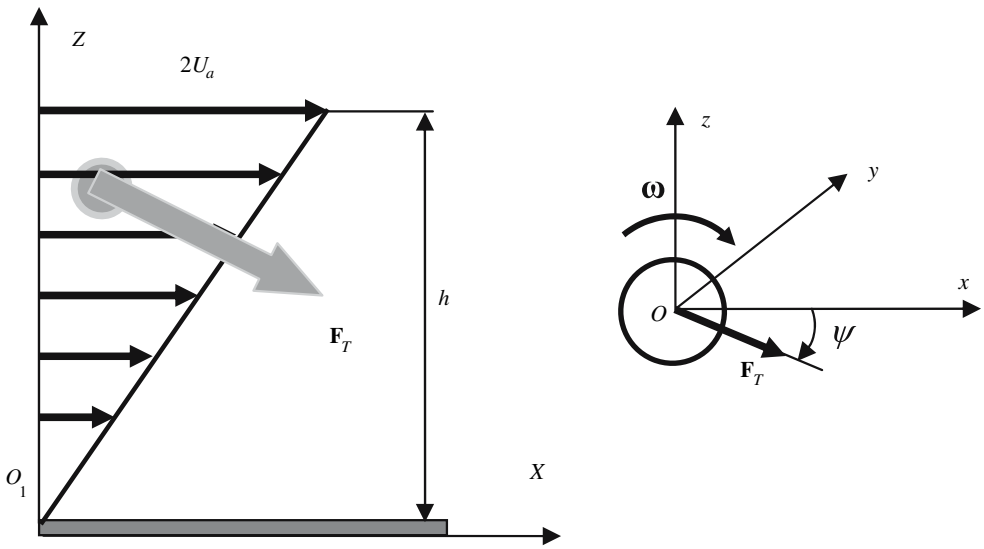


**Fig. 5** A larva in a linear shear flow. The gray circle denotes a larva-particle, and the thick gray arrow indicates the vector of its self-thrust, which rotates due to the larva's rotation

characteristic velocity $U_a$ determine the characteristic time $h/U_a$. For further analysis, where necessary we shall use non-dimensional coordinates and non-dimensional time scaled with these reference values.

Using Eq. 29 to calculate the vorticity gives the following system of differential equations of motion of a larva in a linear shear flow:

$$\frac{d\xi}{d\tau} = 2\zeta + \frac{1}{\lambda}\cos\psi, \tag{30}$$

$$\frac{d\zeta}{d\tau} = -\frac{1}{\lambda}\sin\psi - \overline{V}_t, \tag{31}$$

$$\frac{d\psi}{d\tau} = 1 - \varepsilon\sin\psi, \tag{32}$$

where $\xi = X_O/h$, $\zeta = Z_O/h$, $\tau = U_a t/h$

$$\varepsilon = \frac{gb_C}{6\nu}\frac{h}{U_a}, \tag{33}$$

$$\lambda = \frac{U_a}{V_S}, \tag{34}$$

$$\overline{V}_t = \frac{V_t}{U_a}, \tag{35}$$

and

$$V_t = -\frac{(\rho_p/\rho - 1)D_p^2}{18\nu}g. \tag{36}$$

Consider now a laminar flow in a tube of radius $R$ with an axis directed along the axis $O_1X$ of the fixed in space coordinate system (Poiseuille flow) (Fig. 6). The vector of the fluid velocity in the tube is represented as follows:

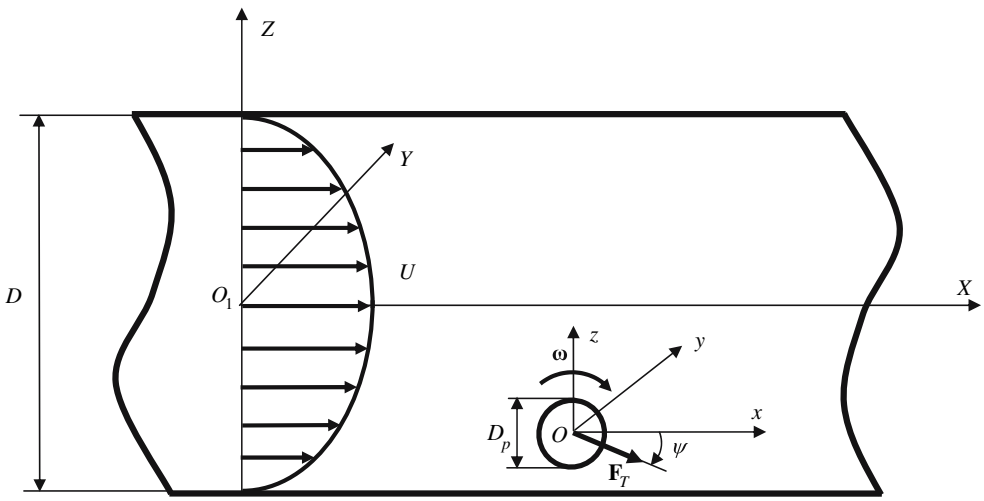


**Fig. 6** Larva in the Poiseuille flow; $D$ is the diameter of a tube or the width of a channel. A rigid particle, which is located below the axis of the tube rotates with a positive angular velocity $\omega$

$$\mathbf{U} = 2U_a\left(1 - \frac{Y^2 + Z^2}{R^2}\right)\mathbf{j}_x. \tag{37}$$

The flow in the plane of symmetry of such a tube is identical to the flow in the two-dimensional Poiseuille channel of width $D = 2R$:

$$\mathbf{U} = 2U_a\left(1 - \frac{Z^2}{R^2}\right)\mathbf{j}_x. \tag{38}$$

For a two-dimensional Poiseuille flow the non-dimensional equations of motion of a larva are the following:

$$\frac{\mathrm{d}\xi}{\mathrm{d}\tau} = 2(1 - \zeta^2) + \frac{1}{\lambda}\cos\psi, \tag{39}$$

$$\frac{\mathrm{d}\zeta}{\mathrm{d}\tau} = -\frac{1}{\lambda}\sin\psi - \overline{V_t}, \tag{40}$$

$$\frac{\mathrm{d}\psi}{\mathrm{d}\tau} = -2\zeta - \varepsilon\sin\psi, \tag{41}$$

where

$$\varepsilon = \frac{gb_C}{6\nu}\frac{R}{U_a} \tag{42}$$

$\xi = X_O/R$, $\zeta = Z_O/R$ and $\tau = U_a t/R$. Note that for the linear shear and Poiseuille flows we use the same notations for the non-dimensional coordinates and time. That should not lead to confusion because in each particular case the meaning of the variables is clear from the context of the problem.

The differential equations of motion of a larva can be solved analytically or numerically. In both cases they must be provided by initial conditions, i.e., by coordinates of a larva and its Euler angles (the pitch angle for a two-dimensional case).

### Randomness of initial conditions

Different initial conditions of the equations of motion of a larva result in different larva's trajectories. Our goal is not only to calculate the trajectories but mainly to estimate the probability of contact, a number. This single number is a functional of all trajectories. However, the initial coordinates of a larva and its Euler angles are unknown because they are random. In the absence of detailed experimental data, we assume that all possible initial coordinates of a larva and its initial Euler angles are random numbers which are distributed uniformly within corresponding physically meaningful ranges (see for instance, Fig. 7). The number of possible trajectories of a larva is infinite. Therefore, in the consequent analysis we illustrate only the most representative of them, those, which allows us to analyze only the principal features of the contact phenomenon.

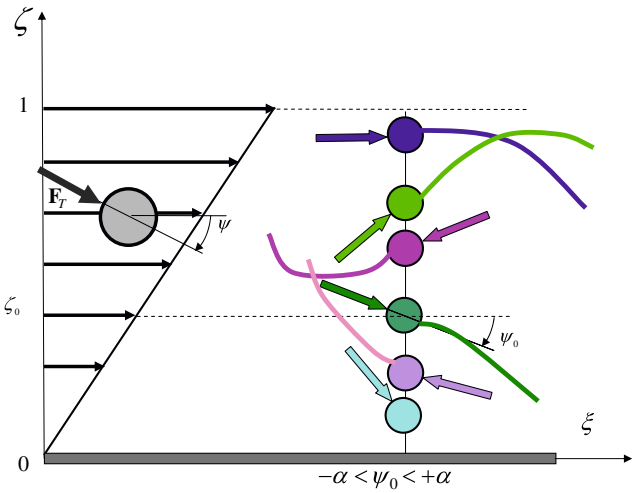


**Fig. 7** Larvae entering a linear shear flow with different coordinates $\zeta = Z_O/h$ and different angles of turn $\psi_0$ ($0 < \zeta < 1$, $-\alpha < \psi_0 < \alpha$, $\alpha < \pi$). Due to the shear each larva rotates and the vector of its self-thrust $\mathbf{F}_\mathrm{T}$ also rotates. *Circles* indicate larvae, the *arrows* connected to the *Circles* indicate the initial directions of the self-thrust, and curves the possible variety of larval trajectories

## Results

### Larval trajectories in a linear shear flow

Within the system of the three differential equations 30–32 consider first the isolated equation 32, which involves parameter $\varepsilon$ given by Eq. 33. This differential equation has a closed form analytic solution, which is not provided here because of its complicity. It follows from this solution that the behavior of the angle of pitch $\psi(\tau)$ depends whether the parameters $\varepsilon$ is larger than one or smaller than one.

For $\varepsilon > 1$ equation 32 has two steady state solutions corresponding to zero angular velocity $\mathrm{d}\psi/\mathrm{d}\tau = 0$:

$$\psi_e = \arcsin\left(\frac{1}{\varepsilon}\right) \tag{43}$$

and

$$\psi_{eu} = \pi - \arcsin\left(\frac{1}{\varepsilon}\right). \tag{44}$$

It can be shown that for the first of them, Eq. 43, the equilibrium is stable and for the second one, Eq. 44, the equilibrium is unstable. A larva can keep the angle of the direction of motion $\psi_{eu}$ only if maintains its orientation in space deliberately, due to certain biotic causes such as responds to light or chemical cues. These processes are excluded from our consideration.

An analytic solution of the equations of motions 30–32 for a larva, which moves in a vertical plane without rotation with an angle of pitch given by Eq. 43 is the following:

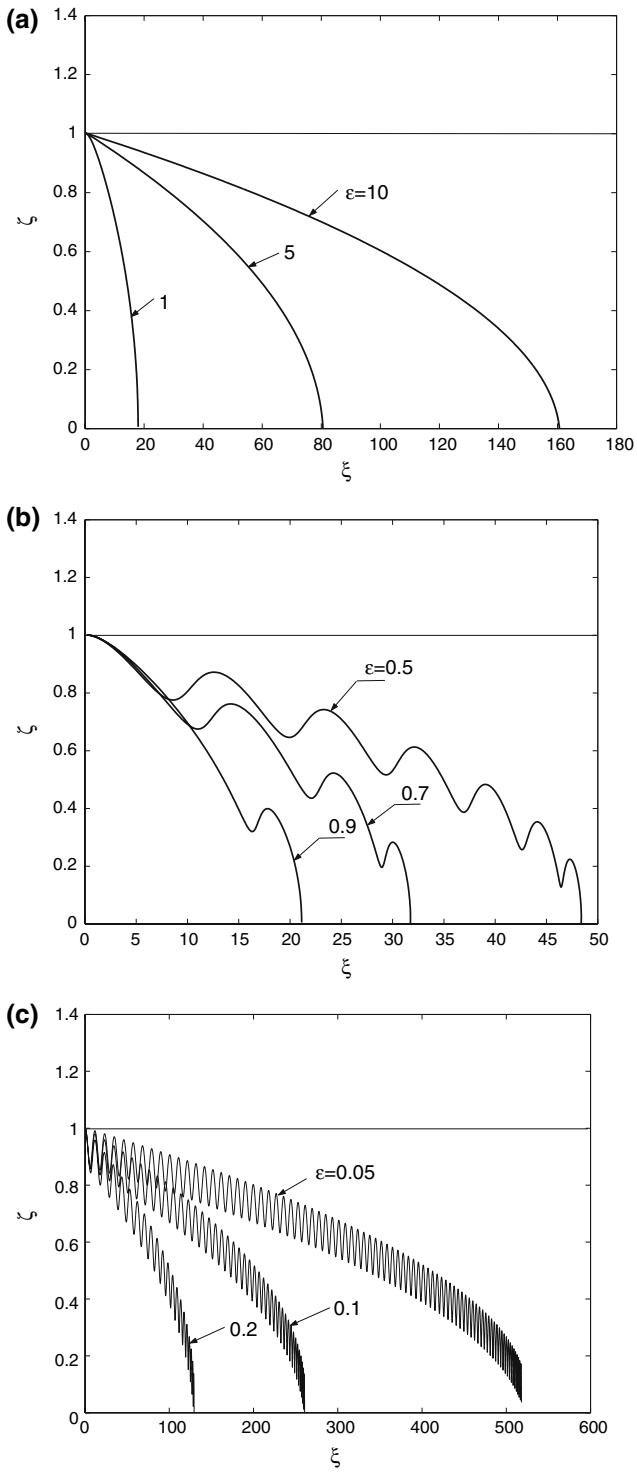


**Fig. 8** Trajectories of a larva in a linear shear flow. The vertical coordinate $Z_O$ and the horizontal coordinate $X_O$ are normalized with the characteristic geometric scale of the flow $h$ yielding $\zeta$ and $\xi$, correspondingly. The gravity force acts towards the bottom $\zeta = 0$. Coordinate $\xi = 0$ correspond to the initial moment of time when the initial angle of turn is zero. For all calculations the ratio $\lambda$ of the flow velocity $U_a$ and the swimming velocity $V_S$ is 15. The type of a trajectory depends on the parameter $\varepsilon$, which represents the ratio of the hydrostatic restoring buoyancy moment and the torque moment induced by the shear stresses on the surface of a larva. Whether contact is possible or not depends on the length of a substrate. **a** For $\varepsilon > 1$ a larva moves without rotation with an angle of pitch $\psi = \arcsin(1/\varepsilon)$. For $\lambda = 15$ the trajectories crosses the bottom in the range $\xi\in(20–160)$; **b** for $0.5 < \varepsilon < 1$ a larva approaches to the bottom in an oscillatory manner. The distance which a larva covers in the horizontal direction prior of making contact is of the same order of magnitude that for $1 < \varepsilon < 5$; **c** for $0.05 < \varepsilon < 0.2$ a larva moves in an oscillatory manner. The distance which a larva covers in the horizontal direction prior of making contact is rather large

$$\xi = 2(\zeta_0 + \frac{1}{2\lambda}\sqrt{1 - 1/\varepsilon^2})\tau - \left(\frac{1}{\varepsilon\lambda} + \overline{V_t}\right)\tau^2, \tag{45}$$

$$\zeta = \zeta_0 - \left(\frac{1}{\varepsilon\lambda} + \overline{V_t}\right)\tau, \tag{46}$$

where $\zeta_0 = Z_O^0/h$ is the initial coordinate of a larva $Z_O^0$ which is scaled with the characteristic length of the problem. From Eq. 46 it is possible to find the time $t_{\text{contact}}$, which is necessary for a larva to reach the bottom if its initial coordinate is $Z_O^0$:

$$t_{\text{conact}} = \frac{Z_O^0}{(V_S \sin\psi_e + V_t)}. \tag{47}$$

From Eq. 47 follows an important conclusion. A larva can be neutrally buoyant or even positively buoyant but nevertheless is can approach the bottom as long as the total vertical velocity $V_S \sin\psi_e + V_t$ is positive. The motion of a larva is driven by its self-propulsion and by two hydrodynamic moments, the torque moment induced by the shear of the flow and by the buoyancy moment, which may eliminate each other. It should be stressed, that in reality the fluid velocity field is inevitably disturbed and a larva will oscillate around the stable equilibrium position with non-zero angular velocity of pitch. We assume that the disturbances are sufficiently large in order to invoke self-propulsion yet sufficiently small not to change the trajectory.

For $\varepsilon < 1$ a larva performs an oscillatory motion, which can be analyzed numerically. Some numerical calculations of trajectories of a larva are shown in Fig. 8 where it is seen for realistic values of the parameter $\varepsilon$ a larva with self-propulsion always reaches the bottom and for an infinitely long substrate contact always takes place, i.e., $P = 1$. However, in many such cases a larva has to travel a relatively large distance in the horizontal direction which sometimes can not be provided in experiments, in particular, in laboratory flumes or tubes. Possibly, that has to be taken into account in comparisons of mathematical models of larval contact with results of experimental observations.

Consider now a larva which approaches to a vertical substrate and moves in horizontal plane. In such a case it is logical to assume that the effective weight of a larva and the buoyancy moment do not influence the process of motion. Assume for simplicity that the boundary layer of a

vertical body can be approximated by a linear boundary layer. In such a case, we can analyze the motion of a larva in a linear shear flow according to equations 30–32 with $\varepsilon = 0$ and $\overline{V_t} = 0$, correspondingly.

Assume that at the initial moment of time $t = 0$ the spatial and angular coordinates of a larva are given by $\zeta_0 = Z_O^0/h$ and $\psi(0) = 0$. Direct analytic integration of Eq. 30–32 for $\varepsilon = 0$ yields the following solution for the coordinates of a larva and its angle of turn:

$$\xi = 2\left(\zeta_0 - \frac{1}{\lambda}\right)\psi + \frac{3}{\lambda}\sin\psi, \tag{48}$$

$$\zeta = \zeta_0 - \frac{2}{\lambda}\sin^2\frac{\psi}{2}, \tag{49}$$

where

$$\psi = \frac{U_a t}{h}. \tag{50}$$

Trajectories of a larva in a linear shear flow, which start the motion with different initial coordinates $\zeta_0$ and zero initial angle of turn $\psi(0)$ are plotted in Fig. 9.

In a linear shear flow, a self-propelled larva performs an oscillatory motion: it rotates with constant angular velocity, and moves not only in the longitudinal but also in the transversal direction across the mean stream. According to Eqs. 48, 49 the condition of contact depends on the initial coordinate $\zeta_0$ and the velocity parameter $\lambda$ given by Eq. 34. From Eq. 49 it follows that if the angular velocity of a larva is relatively small but the self-thrust is relatively large, the larvae will reach the substrate prior to making a full turn. This scenario takes place when $\lambda = U_a/V_S \leq 2$. If the angular velocity is relatively high and the self propulsion force is relatively weak, a larva will make a full turn prior to reaching the bottom, which take place for $\lambda < 2$. The qualitative behavior of a larva in a linear shear flow is illustrated in Fig. 10.

## Probability of larval contact in a linear shear flow

In order to obtain a simple formula for the contact probability $P$, consider first a large number of similar larvae entering the shear flow with the same zero initial angle of pitch $\psi(0) = 0$; and assume that initial coordinates of larvae $\zeta_0$ are distributed within the range (0,1) randomly and uniformly. For the sake of simplicity, it is assumed also that outside the layer of thickness $h$ ($\zeta = 1$) the flow is irrotational and in such irrotational flow a larva moves along streamlines parallel to the fixed wall $\zeta = 0$. To analyze the contact probability, note that, at the moment of contact the vertical coordinate $\zeta(\tau) = 0$.

It is seen from Eq. 49 that for any $\lambda \leq 2$ the trajectory of a larva always crosses or touches the bottom independently

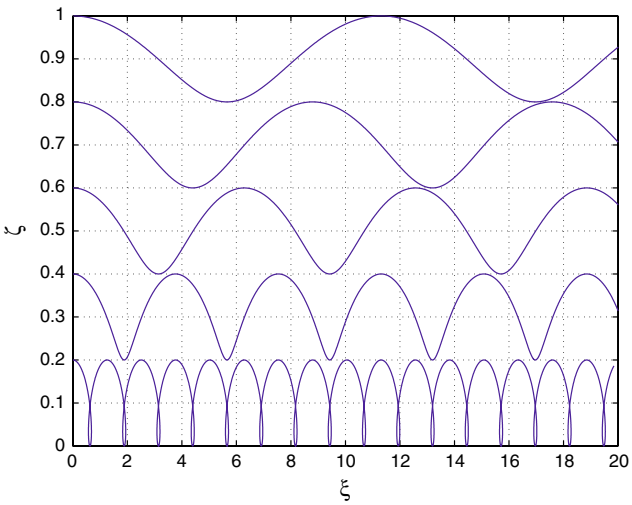


**Fig. 9** Trajectories of a larva with a zero metacentric height moving in a linear shear flow. The fluid velocity at $\zeta = 1$ is constant, at $\zeta = 0$ it is zero. A larva starts the motion with different initial coordinates and zero angle of pitch. In this particular example, the velocity parameter $\lambda = U_a/V_S$ is equal to 10. A larva with initial coordinates $\zeta_0 = Z_O^0/h > 0.2$ does not reach the bottom; whereas a larva with initial coordinates $\zeta_0 = Z_O^0/h \leq 0.2$ does reach the bottom. In this example, the vorticity has a constant sign and rotates a larva in the same direction

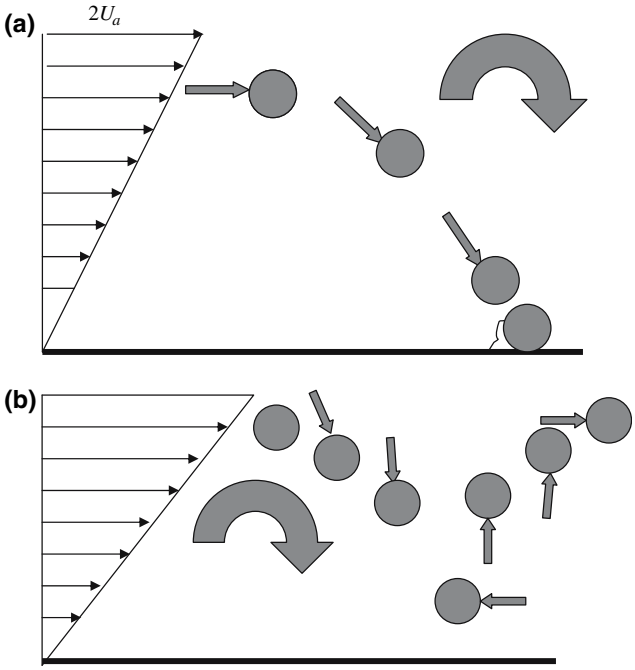


**Fig. 10** Trajectories of a larva with a zero metacentric height moving in a linear shear flow. The fluid velocity at $\zeta = 1$ is constant, at $\zeta = 0$ it is zero. **a** A larva reaches the bottom; **b** a larva makes a full turn prior of reaching the bottom. *Circles* indicate the consequent positions of a larva, the *straight gray arrows* signify the direction of thrust and the *curved gray arrow* the direction of the rotation of a larva. Type (**a**) motion takes place for $\lambda = U_a/V_s \leq 2$; type (**b**) motion takes place for $\lambda > 2$

on the value of the initial coordinate $\zeta_0$, which means that contact always takes place and hence $P = 1$. For $\lambda > 2$, the trajectory of a larva crosses or touches the substrate only if $\zeta_0 \leq 2/\lambda$. In non-dimensional coordinates the thickness of the linear boundary layer (or the width of the Couette channel) is one. For a sufficiently large number of larvae distributed uniformly within the total range [0,1] the probability of contact can be determined as the ratio of the length of the segment [0, $2/\lambda$] and the length of the whole segment [0, 1] yielding the probability of contact as $P = 2/\lambda$. The above results can be summarized in the following remarkably simple form:

$$P = \begin{cases} 1 & \text{for } \lambda \leq 2, \\ 2/\lambda & \text{for } \lambda > 2. \end{cases} \quad (51)$$

From Eq. 51, it follows that for a given swimming velocity of larvae the probability of contact decreases as the characteristic flow velocity increases. In most of available experiments with larvae attaching in tubes the dependence of the probability of settlement on the characteristic flow velocity is similar. Starting from the work of Crisp (1955), it is common to explain this experimental fact by the longitudinal viscous hydrodynamic force acting on a larva in the moment of attachment. It is believed that this force is associated with the wall shear stress. We suggest here a different additional explanation. Our analysis shows that the decrease of the attachment probability can be caused by the kinematics of contact, not only by wall shear stress.

The above results were obtained under the assumption that all larvae enter the vortical flow with the same zero initial angle of pitch. In reality not only the initial coordinates but also the initial angles of pitch are random. To verify the robustness of the mathematical model to variations in the initial angle of pitch, assume that each $i$-th larva enters the vortical flow with an angle of pitch $\psi_{0i}$ ($i$ = 1,2, ...) and that all such angles are distributed randomly and uniformly within a certain range $[-\alpha, \alpha]$; $\alpha = 0$ corresponds to the vector of the self-thrust pointing in the flow direction and $\alpha = \pi$ to the vector of the self-thrust pointing against the flow direction.

The mathematical analysis of the contact probability for $\alpha \neq 0$ is given in Appendix I, formulas I.2–I.3. Plots of these formulas are shown in Fig. 11, which illustrate that the initial angle of pitch does not drastically influence contact probability. In this sense formula 51 is robust.

## Larval trajectories in a Poiseuille channel with vertical walls

The trajectory of a larva in a plane Poiseuille flow is described by equations 39–41 which have no an analytic solution but can be solved numerically for various initial conditions and values of the problem parameters. Examples of trajectories of a neutrally buoyant larva with zero metacentric height are plotted in Figs. 12–14. The influence of the initial coordinate and of the initial angle of pitch on the trajectory of a larva is illustrated in Fig. 12. The influence of the flow parameter $\lambda$ on the type of a trajectory of a larva is illustrated in Fig. 13. Typical trajectories of a larva are plotted in Fig. 14.

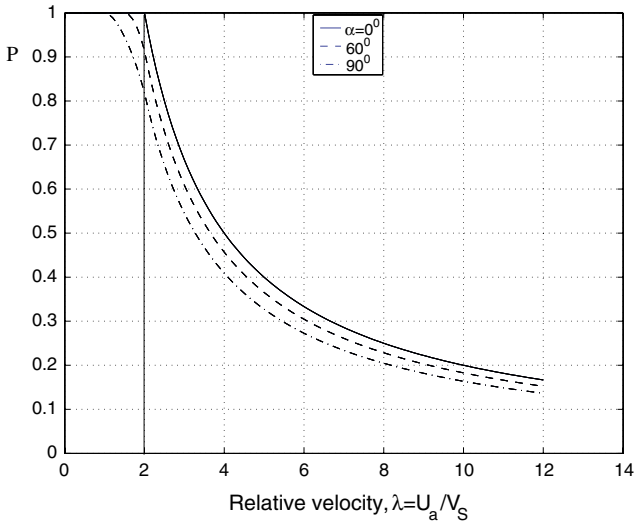


**Fig. 11** Probability of larval contact in a linear shear flow with the wall $\zeta = 0$ where the fluid velocity is zero (on the line $\zeta = 1$ the fluid velocity is constant). Larvae are neutrally buoyant, the metacentric height is zero, different lines pertain to different ranges of the initial angles of pitch distributed randomly in the range $-\alpha < \psi_0 < \alpha$. The values of $\alpha$ do not influence the results drastically. In the range $0 < \lambda < 2$ the contact probability attains the maximal possible value and then decreases asymptotically as $\lambda$ increases. That means that for a given larvae swimming velocity the contact probability is negatively correlated with the characteristic flow velocity

In would be interesting to compare the simulated trajectories of larvae and those measured experimentally in a linear shear or plane Poiseuille flows. Unfortunately, we are not familiar with such experiments data. However, the flow between two coaxial cylinders with a small the gap between them reproduces roughly the flow between two infinite parallel plates. Motion of larvae in a flow between two coaxial cylinders was observed by Pasterank et al. (2004).

According to the experimental results by Pasternak et al. (2004) larvae in a laminar flow between two cylinders move along oscillatory trajectories with amplitudes depending on the flow parameter $\lambda = U_a/V_S$ (Fig. 15a,b); whereas small passive particles move along a straight line (Fig. 15d). For relatively small ratios of the flow parameter $\lambda < 0.8$ the amplitudes of oscillations are large and contact takes place; for faster flows, for lager values of the flow parameters $\lambda > 0.83$ the amplitudes of oscillations are

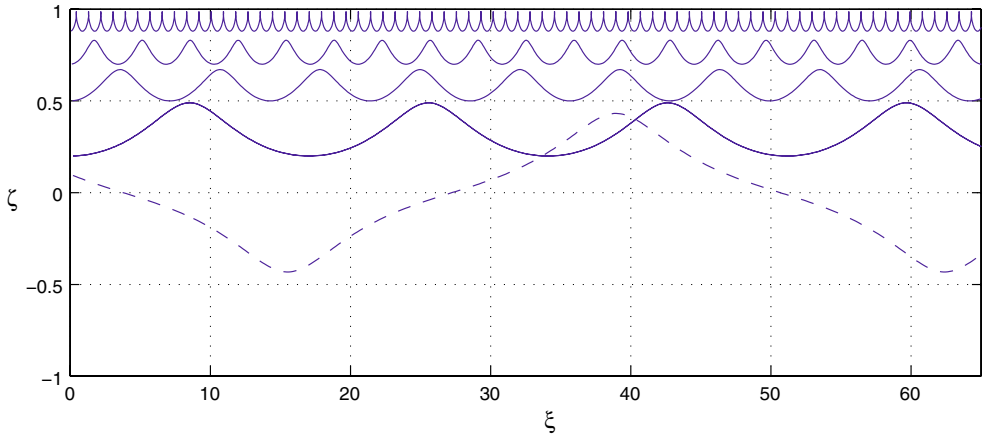


**Fig. 12** Trajectories of a larva in a Poiseuille channel of width $D = 2R$ ($\xi = X_O/R$ , $\zeta = Z_O/R$ ). Due to the symmetry of the flow only positive initial coordinates of a larva are considered. The fluid velocity is zero at the walls $\zeta = \pm 1$. All calculations are performed for the same velocity parameter $\lambda = U_a/V_S = 10$. The larva is neutrally buoyant and its metacentric height is zero. The solid lines represent a larva entering the flow with different initial coordinates but with the same zero initial angle of pitch. A larva performs an oscillatory motion above its corresponding initial coordinate. Only a larva with an initial coordinate $\zeta > 2/\lambda$ may reach the wall. If the initial pitch angle is non-zero then a larva may oscillate around the axis of the channel moving with an angular velocity, which changes the sign according to the sign of the flow vorticity. For instance, the dashed line pertains to a larva, which starts the motion in a channel with an initial coordinate $\zeta_0 = 0.1$ and an initial angle of pitch $\psi_0 = 40^o$. It performs oscillation around the longitudinal axis. It is interesting to compare the trajectories of larvae in a linear shear flow (Fig. 9) and in the two-dimensional Poiseuille flow. In a linear shear flow a larva moves towards the lower wall and in the Poiseuille flow towards the upper wall, because the sign of the vorticity of these two flows is the opposite if we consider a larva with a positive initial coordinate $Z_O$. In the linear shear flow a larva rotates in a clockwise direction and in the Poiseuille channel it rotates in the counter-clock direction

small, and larvae do not make contact. Such patterns of motion are in full qualitative agreement with theoretical results presented in this paper (Fig. 14). It is interesting to note that in still water the trajectories of larvae are drastically different from those in the stream (Fig. 15c), a fact that has been discussed by Butman et al. (1988).

## Probability of larval contact in a plane Poiseuille flow

The calculations of contact probability for the plane Poiseuille flow are given in Appendix II, Eqs. II.5–II.6. Below, we provide only a simple formula for the probability of larval contact when all initial coordinates of larvae represent random numbers distributed uniformly across the channel and when all initial angles of pitch are zero:

$$P = \begin{cases} 1 & \text{if } \lambda \leq 2 \\ 1 - \sqrt{1 - 2/\lambda} & \text{if } \lambda > 2 \end{cases}. \tag{52}$$

For the case when the initial angles of pitch vary randomly and uniformly in the range of given angles $|\alpha| \leq \pi$, the contact probability as a function of the flow parameter $\lambda$ is plotted in Fig. 16. Similarly to the case of a linear shear flow, formula 52 is robust, i.e., contact probability is not affected drastically by the range of the initial angles of turn.

Comparison of Figs. 11 and 16 shows for both, a linear shear and the plane Poiseuille flows the contact probability is a decaying function of the ratio of the characteristic flow velocity and the swimming velocity. This is not surprising because in both cases contact results from the same physical reasons, the vorticity, rotating larvae and their self-propulsion, which changes the direction of action due to the rotation.

## Larval motion in a laminar tube flow

In a tube, the rotating vector of the self-thrust does not remain in the same plane, thus leading to a three-dimensional motion of the larva. The three-dimensional trajectories can be found as a numerical solution of the equations of motion 6–7 and 24–25. An example of the computed numerically typical trajectory of a larva in a tube is shown in Fig. 17. From the results of systematic numerical computations, it follows that in a laminar tube flow a larva undergoes an oscillatory motion of a helix-like type, and that the parameters of the trajectory strongly depend not only on the ratio of the flow velocity and the larva's swimming velocity but also on the random initial conditions of the problem, i.e., on the two initial coordinates ($X_O$, $Y_O$) and Euler angles, respectively.

In order to calculate the probability of contact in a tube Monte-Carlo method is used here (Sobol 1994). The method is based on considering a multitude of trajectories of larvae with different random initial conditions and by

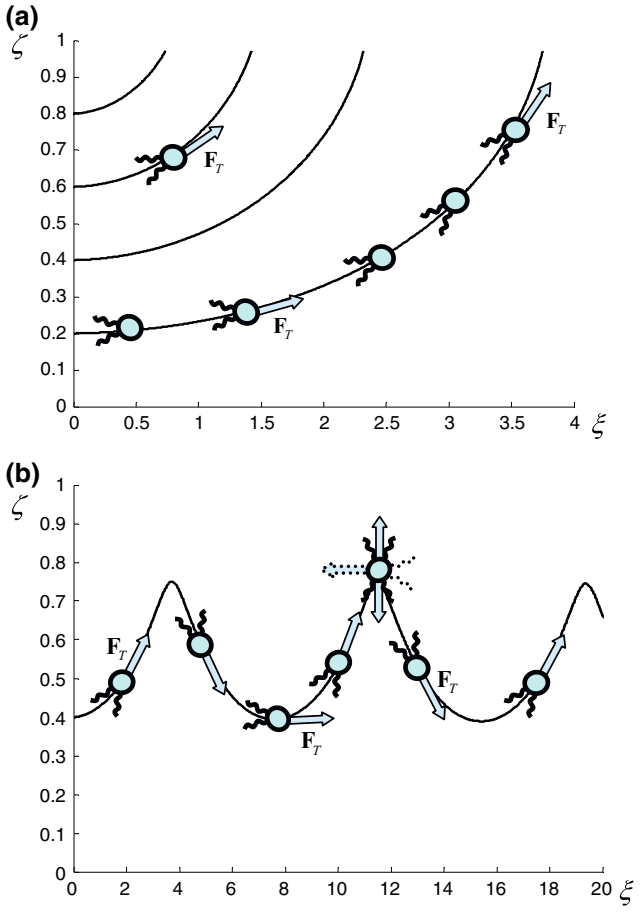


**Fig. 13** Trajectories of a larva in a Poiseuille channel of width $D = 2R$ for different values of the flow parameter $\lambda = U_a/V_S$ ($\xi = X_O/R$, $\zeta = Z_O/R$). Due to the symmetry of the flow only positive initial coordinates of larvae are considered. The *circles* indicate a larva, *arrows*—the vectors of the self-thrust and its altering directions. **a** $\lambda = 1$, $\psi_0 = 0$—a larva reaches the wall; **b** $\lambda = 4$, $\psi_0 = 0$—a larva makes a full turn prior to reaching the wall

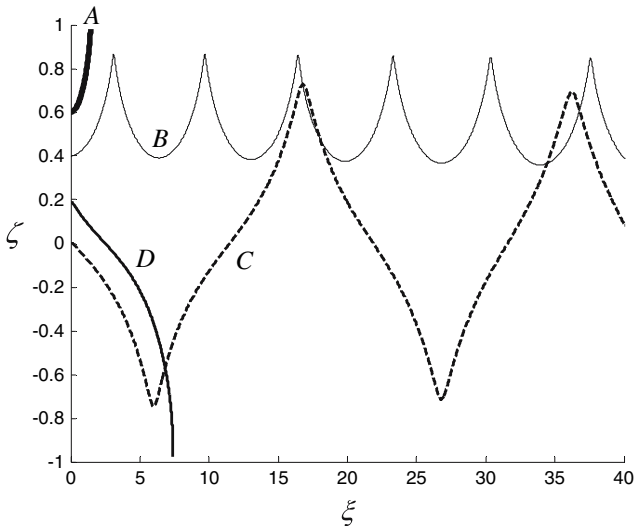


**Fig. 14** Typical trajectories of a self-propelled larva in the Poiseuille channel. Cases *A* and *C* pertain to $\lambda = U_a/V_S \leq 2$; *B* and *D* to $\lambda = U_a/V_S > 2$. *A* A larva starts the motion above the axis of the channel with zero initial angle of turn and rotates with an angular velocity that is determined by the flow vorticity. Due to the rotation, the vector of the self-thrust also rotates and pushes the larva towards the upper wall. The larva reaches the wall prior to making a full turn. *B* A larva starts the motion with zero initial conditions and makes a full turn prior to reaching the wall. *C* A larva starts the motion close to the axis of the channel with a non-zero angle of turn. The self-thrust moves the larva toward the lower wall and it enters the area of the flow which rotates it in a counter-clock wise direction. The rotating vector of self-thrust changes the direction toward the upper wall and moves the larva there. *D* A larva starts the motion above the axis of the channel but reaches the lower wall because the initial angle of turn is relatively large and the magnitude of the flow vorticity is insufficient to change the direction of the self-thrust in the direction toward the upper wall

verifying how many of them cross the wall of the tube. The principles of generation of random initial conditions for a tube are given in Appendix III.

The algorithm for calculating of the contact probability of larvae in a tube is as follows: for each given $\lambda = U_a/V_S$ the equations of motions motion of a larva 6–7 and 24–25 with random initial conditions are solved numerically $N$ times; the ratio of $n$ simulation, where contact took place, and the total number of $N$ runs determines the seeking probability, $P = n/N$. In practical computations, the number of simulated larvae was taken as 2,000. This number has been found by increasing the initial number $N = 200$ by 200 until the result of computation for two maximal consequent $N$ gave close results with a relative error within 10% (for $\lambda < 5$ it does not exceed 5%). Giving that in available experiments the accuracy of the measured settlement probability is limited and that computations of 2,000 trajectories of larvae for each $\lambda$ are time consuming, such an error can be considered as quite permissible for purely qualitative comparisons of experimental and theoretical results.

Prior to formulating the criteria of larval contact in a tube, note that so far we have considered a larva as a point object. However, due to the attachment devices of propagules they initiate contact when the distance $d$ between the wall and the center of mass of a larva is estimated roughly as $D_p/2 < d < 3D_p/2$ (Abelson and Denny 1997). In such a case, the criterion of contact is described by an inequality

$$\frac{\sqrt{Y_O^2 + Z_O^2}}{R} > 1 - \delta, \tag{53}$$

where $\delta = d/R$ is a small quantity varying in the range $D_p/D < \delta < 3D_p/D$. If Eq. 53 is satisfied then larvae do contact the wall; otherwise contact does not takes place. In the numerical simulation presented here, the computations of larva trajectories were continued until contact took place or, alternatively, until the larva had traveled along the tube a distance not less than about 200 tube diameters, which is the ratio defining the physical length of a tube in most of the relevant experiments. The results of systematic

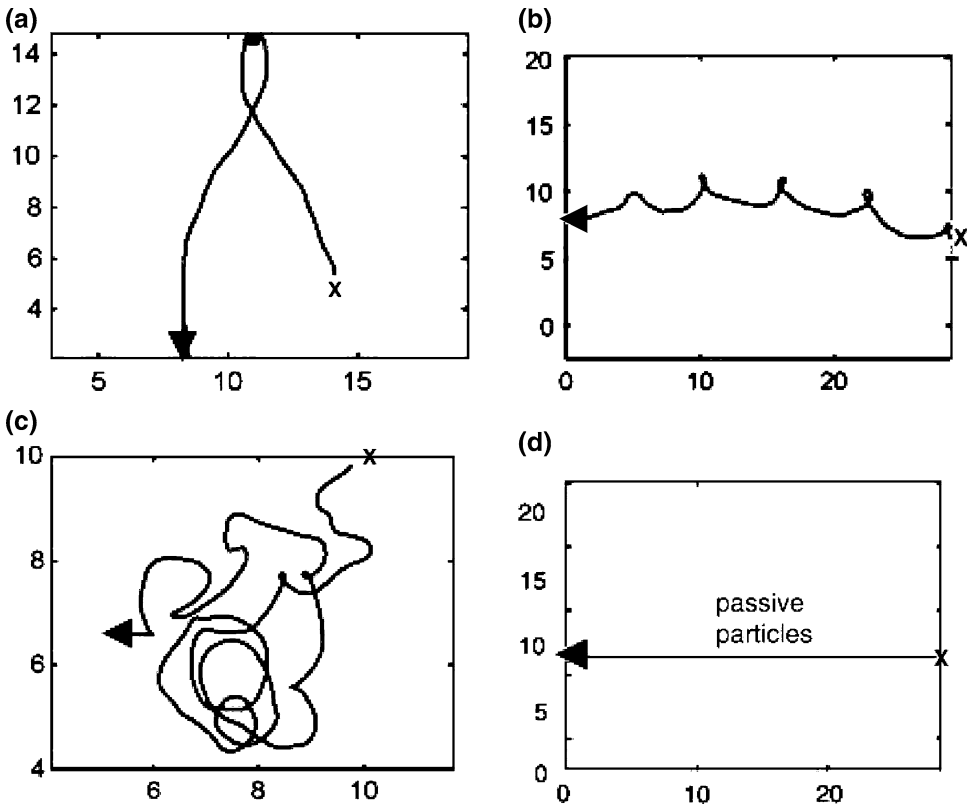


**Fig. 15** Typical trajectories of larvae of *Hetersacuss dolffusi* in a plume in the absence of host (from Pasternak et al. 2004 by permission of Oxford University Press). Trajectories begin at the *X* and end with a *small arrow*. *Horizontal* and *vertical* axes are given in mm. **a** Larva in flow, $\lambda = U_a/V_S \leq 0.8$; **b** larva in flow, $U_a/V_S > 0.8$; **c** larva in still water; **d** passive particle in flow. The average length of larvae of *H. dolffusi* in the experiment was about 270 μm. Thus, the amplitudes of the trajectory oscillations exceed this characteristic length by orders of magnitude. The type of trajectories (**a**) and (**b**) correspond to those shown in Fig. 14, curves *B* and *C*. Note that trajectories of a passive particle and a larva in still water differ drastically from those demonstrated by living larvae in a stream

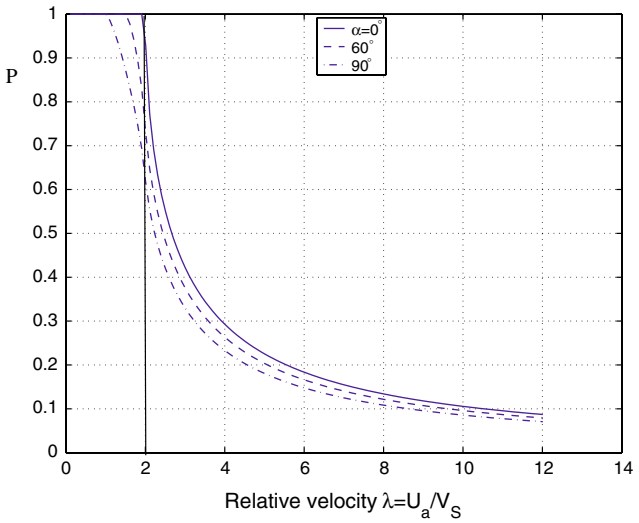


**Fig. 16** Probability of larval contact in the Poiseuille channel. Larvae are neutrally buoyant, the metacentric height is zero, different lines pertain to different ranges of the initial angle of pitch which is distributed randomly in the range $-\alpha < \psi_0 < \alpha$. The values of $\alpha$ do not influence the results drastically. In the range $0 < \lambda < 2$ the contact probability attains the maximal possible value and then decreases asymptotically as $\lambda$ increases. That means that for a given larvae swimming velocity the contact probability is negatively correlated with the characteristic flow velocity

numerical computation show that if the flow parameter $\lambda$ varies between 0 and 15 then larval contact in a laminar tube flow takes place within 50 tube diameters.

The results of systematic numerical computations show that the qualitative behavior of the contact probability for a linear shear, the plane Poiseuille, and the three dimensional Poiseuille flows is similar, i.e., for all the three flows the contact probability is a decaying function of the flow parameter $\lambda$.

In the absence of experimental measurement of contact rates for the three studied flows we compare our theoretical results with experimental measurements of the attachment probability. Although the contact probability is only an upper bound of the attachment probability, the correlation (positive or negative) between the two probabilities is of great interest.

Qian et al. (1999) observed the attachment of *Hydroides elegans* and *Bugula neritina* in 2 m long tubes for laminar and turbulent flow regimes. We compare the results of the mathematical simulations with the experimental results for the laminar flow.

In our numerical simulations the larvae diameters and their swimming velocities were taken from Qian at al. (1999) for *Hydroides elegans* and from Wendt (2000) for *Bugula neritina*.

The *B. neretina* is close to a spheroid with an aspect ratio of about 1.1. Its equivalent diameter is about 243 μm, the swimming velocity is close to 0.47 cm/s and the Reynolds number is about 1.2. For such Reynolds numbers the Stokes' formula for the drag of a small sphere underestimates its value by 15%. Given the nature of the problem

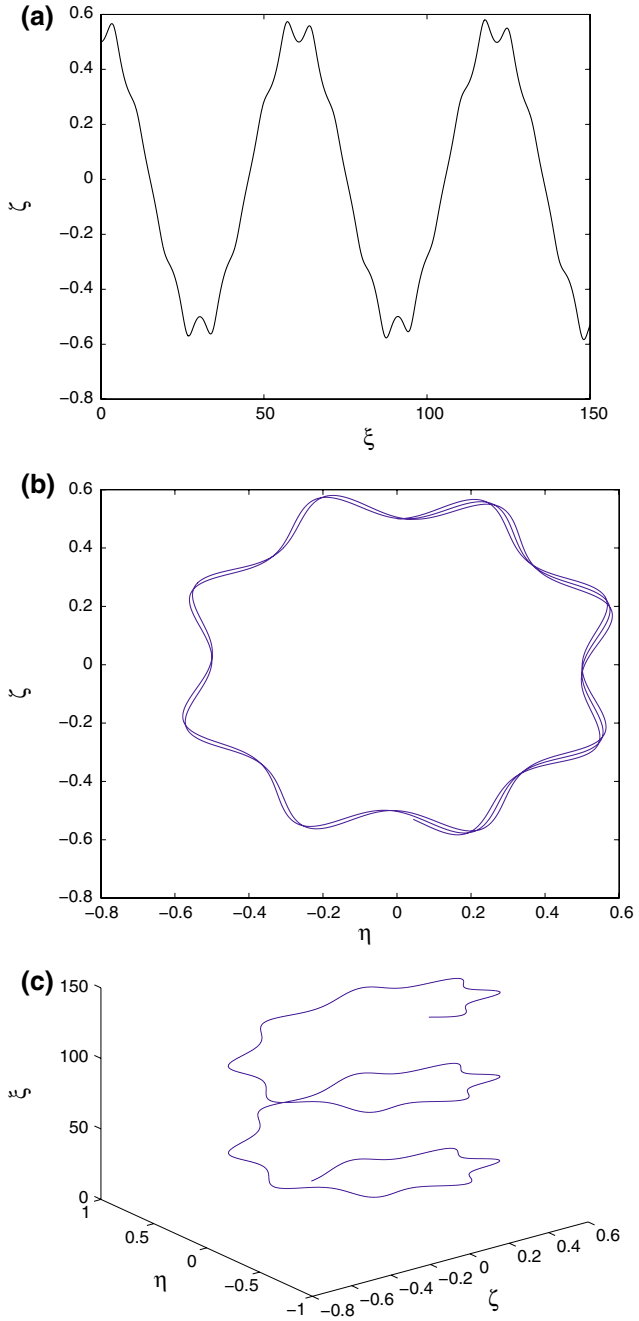


**Fig. 17** A typical three-dimensional trajectory of a larva in a circular tube of radius $R(\xi = X_O/R,\ \eta = Y_O/R,\ \zeta = Z_O/R)$, $\lambda = U_a/V_S = 10$). **a** The projection of the trajectory on the $O_1XZ$ plane; **b** the projection of the trajectory on the $O_1YZ$ plane; **c** three-dimensional trajectory

for *B. neretina* such an error can be considered as permissible for qualitative comparisons.

The ratio of the length and beam of the approximately spheroidal *H. elegans* is about two (Walters et al. 1997). For *H. elegans* with an equivalent diameter of 163 μm and swimming velocity of about 1 cm/s the Reynolds number is about 1.6. Concerning slender species *H. elegans*, it was already mentioned above that an elongated elliptical particle moves in the tube flow along an oscillatory trajectory even without self-propulsion. Whether such a particle may contact the wall of a tube for small values of its effective weight and what is the probability of contact in this case is a matter for detailed analysis, which is beyond of the scope of the present study. Although in our theory, we consider spherical larvae, we find it instructive to compare the theoretical and experimental results for *H. elegans* because it is possible that the self-propulsion force influences larval trajectories more significantly than their non-sphericity.

It should be stressed that we do not intend to compare the experimental and theoretical results quantitatively. Numerous uncertainties of the problem parameters, the individual behavior of a larva, its latency to react to flow variations, its age make this task difficult. Therefore, as it was already stressed, we compare the theoretical and experimental results only qualitatively.

The theoretical results and the experimental data are compared in Fig. 18. For both species the plots demonstrate an obvious correlation between the probabilities of the two different phenomena, the attachment (experiment) and the initial contact (theory), except in the range of low ratios $\lambda = U_a/V_S$.

In the range of the flow parameter $\lambda > 2$ the theoretical values are somewhat higher than the experimental ones. Several reasons may explain this discrepancy. First, a larva making contact can leave a substrate without attaching because of high shear stress on the wall. In our work we assumed that the length of the tube is infinite; whereas in experiments the tubes were 2 m in length. Although in those experiments most of the settled larvae were found within the first 0.5 m of the tube, it is possible that some of larvae, especially those which had explored the substrate by making several contacts, left the tube because of the limited time of residence.

In the range $\lambda < 2$, where the theoretical values of the contact probability are maximal, the experimental values are uncertain and vary between zero and one. Paradoxically, this discrepancy may be considered as an argument in favor of the proposed theory rather than as an obstacle to it. According to the mathematical model developed here larvae do not attach if they do not use their self-propulsion abilities. According to observations of Crisp (1955) there is a range of low shear rates where larvae do not use thrust and do not attach. On the axis of the tube the vorticity is zero and it is possible that larvae, which are located close to the axis, rotate with such a small angular velocity that it does not trigger the self-thrust. We have assumed, however, that larvae use their self-thrust for even very small values of the flow vorticity. That may be the possible cause of the discrepancy between the theoretical results and experimental measurements in the range $0 < \lambda < 2$.

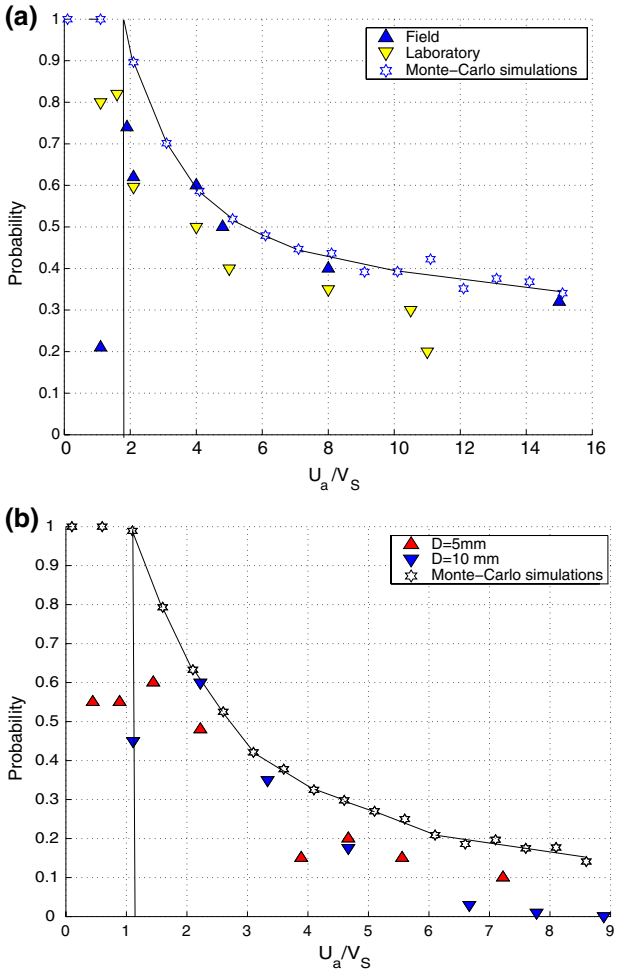


**Fig. 18** The probability of attachment (experiment) and the probability of contact (theory) for **a** *B. neritina* and **b** *H. elegance*. The diameter of the experimental tubes is $D = 10$ mm. The theoretical and experimental results are compared in the range of experimental flow velocities corresponding to the laminar regime ($U_a < 10$ cm/s). The contact probability is calculated for discrete values of the flow parameter $\lambda$ with a step $\lambda = 1.0$. It is assumed that larvae are neutrally buoyant and their metacentric height is zero. The results of mathematical simulations by Monte-Carlo method are depicted by stars, which are connected by a solid line. The accuracy of Monte-Carlo simulations is within 10%. The length, beam and the swimming velocity of *B. neritina* are estimated as 271 μm, 231 μm and 0.47 cm/s, respectively. The ratio of the diameter of larvae to the radius of the tube is estimated as $\delta = 0.035$. The length, beam and swimming velocities of *H. elegance* are estimated as 275 μm,125 μm and 1 cm/s, respectively, $\delta = 0.006$. In the area between the vertical axis $\lambda = 0$ and vertical lines $\lambda = 1-2$ the experimental values of the attachment probability are uncertain because larvae may or may not use the self-thrusts

## Discussion

We made an attempt to explain larval contact in laminar flows as a result of the combined action of the flow vorticity and of the self-propulsion of a larva. We studied larval contact in three types of laminar flows: in a two-dimensional linear shear flow, in the two-dimensional Poiseuille channel, and in the three-dimensional Poiseuille tube. According to the presented here mathematical model the probability of contact is a decaying function of the ratio of the characteristic flow velocity and swimming velocity of larva.

The simulated values of the contact probability for a tube flow are in satisfactory qualitative agreement with experimental measurements of the attachment probability. Most experimental observations confirm the decay of attachment rate as the flow velocity increases. The common explanation of this experimental fact is well known. It is believed that shear stress on the body of a larva after it made contact is strongly associated with the wall shear stress. Because in a tube flow the wall shear stress is proportional to the corresponding wall rate of shear, Crisp (1955) suggested that the probability of larval settlement is related to the rate of shear.

However, in tube flows the rate of shear, the shear stress and the vorticity are proportional to the same gradient of the axial velocity calculated in the radial direction. This similarity can easily obscure the actual physical relation between the contact and attachment phenomena. In our interpretation, they are related—but governed by two different hydrodynamic characteristics of the flow—one by the flow vorticity, determining contact, and the other one by the wall shear stress that is responsible for the ultimate attachment.

The mathematical model is formulated here for laminar flows. It is likely, however, that it can be applied to certain (not all) natural flows. The corresponding examples are given in Figs. 19–21.

According to the main assumption of our work, to attach, at least in laminar flows, larvae must use their self-thrust. In such a case a question arises how propagules without motility, e.g., many of almost spherical aglal spores can colonize vertical substrates and, in particular, rocky shores (Denny and Shibata 1989). The most likely explanation is that turbulent mixing will cause larval transport. Our model is not intended to describe such processes.

Another interesting question is how larvae attach in still water, a case that can be reproduced only under laboratory conditions. Certain types of larvae even in still water are able to reach a substrate by employing gravitational sinking or self-propulsion. However, larval behavior in still water is drastically different from that in flow (Butman and Grassle 1988; Pasternak et al. 2004) and, obviously, our mathematical model is not intended to describe such process either.

Our mathematical model is restricted by larval forms with a small degree of non-sphericity and with hydrodynamically smooth surfaces. Real larvae are non-spherical

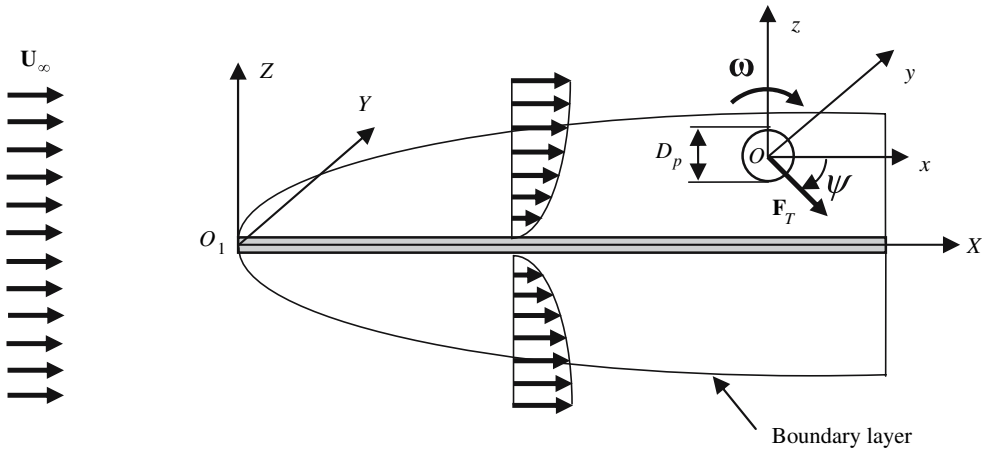


**Fig. 19** Larva-particle in the laminar boundary layer of a thin plate. The velocity profile in the boundary layer is a nonlinear function of the coordinate normal to the plate. It can be approximated by a linear dependence, yielding a linear shear layer, or by a parabola relating to the velocity profile in Poiseuille flow. The boundary layer in the vicinity of the leading edge is laminar although at the rest of it the flow may be turbulent. The critical Reynolds number when the laminar flow on a plate turns into a turbulent flow is of an order of $3 \times 10^5$ which is considered as a lower bound of the critical Reynolds number. For flows with very small external perturbations the critical Reynolds number can be higher by an order of magnitude. *Examples*. For the fluid velocity of an order of 3 cm/s the length of the laminar region on a flat plate is of an order of 10 m. The thickness of the boundary layer on such a plate after the first 11 cm from the leading edge is more than 1 cm. This is by two orders of magnitude higher than the size of a larva with a typical length of 100 μm. The laminar boundary layer of a flat plate is a very good approximation of the boundary layer of a slender body

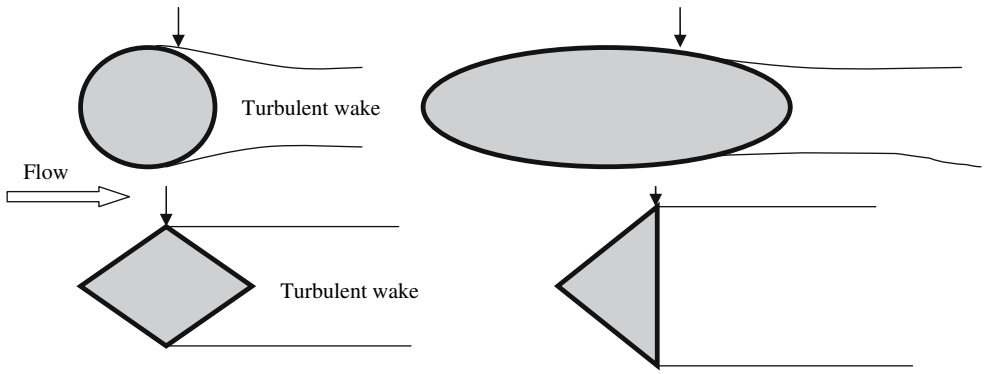


**Fig. 20** Bodies with a well-defined flow separation area which is indicated by a *thin black arrow*. The *thick white arrow* on the left shows the direction of the ambient flow. The wakes of the bodies are turbulent; whereas the boundary layer on their front upstream part may be laminar. *Examples*. The critical Reynolds number for a smooth sphere when the flow on its downstream rear part becomes turbulent is about $3 \times 10^5$, which corresponds to the sphere diameter of an order of 5 m and an ambient fluid velocity of an order of 6 cm/s. For a slender smooth body like an ellipsoid with an aspect ratio lager than six the critical Reynolds number is of order of $10^6$, which corresponds to the length of a body of about 16.5 m and to the fluid velocity of about 6 cm/s. Even on relatively large bodies the flow may be fully laminar or laminar on its upstream front parts. Of course, roughness of the body, non-steadiness of the flow and external turbulence may change these estimates but, nevertheless, the order of magnitude of the above numbers is generally accepted (Schlichting 1979)

and non-smooth. As long as we remain within the hydrodynamics of low Reynolds numbers, the slenderness of larvae and small variations of their form can still be included into the mathematical model (Happel and Brenner 1983). However, it is likely that analysis of the dynamic of a slender, buoyant and self-propelled larva of an arbitrary form which moves in a vortical laminar along a curvilinear trajectory can be tackled only by solving numerically the full nonlinear Navier–Stokes equations.

The analysis presented here is carried out for laminar flows. For turbulent flow with high turbulent intensity and low mean flow velocity the model proposed here can not be applied directly. However, as it was already discussed above many relevant natural flows, where larvae settle, can be considered as partially laminar or can be characterized by a low level of turbulence. In this respect the basic assumption of our model are valid although obviously restricted.

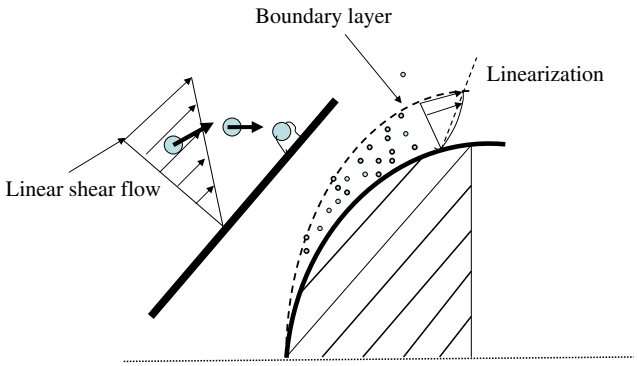


**Fig. 21** Approximation of a boundary layer velocity profile by a linear velocity profile. *Circles* denote larvae in a linear shear flow and in a boundary layer of a body of general geometry. Since both flows are vortical, the kinematic behavior of larvae in a boundary layer and in a linear shear flow are expected to be similar

In our work, we separated biotic and abiotic factors, although it is known that some larva may respond to light and gravity by correcting their body orientation. In this case the effect of vorticity on the body rotation and its trajectory may be less significant.

It must be stressed that we did not solve the problem of contact phenomenon in its entire complicity. We did not intend to do it. We have chosen only one important aspect of the problem and studied it by using a simplified hydrodynamic model of the contact phenomenon. More theoretical and experimental works are needed in this direction.

In conclusion we wish to mention another important implication of our work, which was suggested by one of the *anonymous reviewer of the manuscript*. Examples of laminar flows, in which self-propelled organisms are small compared to the geometrical scale of the shear flow, include bacteria and protists in biofilms, and bacteria or motile parasites in internal vessels of other organisms.

**Acknowledgments** The Italian Ministry of Land and Environments (grant 2004/2006) supported this study. The authors are grateful to A. Abelson for constructive discussions and his valuable comments, to L. Shemer for his useful advice on the Monte-Carlo simulations and to N. Paz for her editorial assistance. The manuscript of this work was read by four anonymous reviewers whose comments are greatly appreciated by the authors.

## Appendix I

In this Appendix, we analyze the contact probability for a linear shear flow Eq. 29 bounded by a fixed wall with a coordinate $Z = 0$. The flow can be unbounded from above, it can represent a flow between two walls, when one of them moves or it can be viewed as linear boundary layer. In all the three cases the characteristic linear scale of the problem is $h$ and the characteristic velocity is $U_a$. These two parameters allow us to define the non-dimensional time as $\tau = U_a\, t/h$ and the non-dimensional coordinates of the larva $\xi = X_O/h$ and $\zeta = Z_O/h$, correspondingly. In non-dimensional coordinates the boundaries of the Couette flow are represented by lines $\zeta = 0$ (lower boundary) and $\zeta = 1$ (upper boundary).

The dimensionless equations of motion Eqs. 30–32 can be expressed in a form of a parametric dependence as

$$\zeta = \frac{2}{\lambda}\left(C - \sin^2\frac{\psi}{2}\right), \tag{I.1}$$

where $C$ is a constant of integration, which is determined by initial conditions $(\zeta_0, \psi_0)$.

Expression I.1 represent an infinite number of curves because the number of constants of integration is also infinite. If we plot all such curves $\zeta = \zeta(\psi,C)$ together (Fig. 22) we obtain a diagram which can be used for analyzing the contact probability. For each particular constant $C_i$, we have a particular curve $\zeta_i = \zeta(\psi,C_i)$. The correspondence between the constant and the curve (or the curve and the constant) is one-to-one.

Each curve of the diagram in Fig. 22 represents a coordinate of a particle $\zeta$ as a function of its angle of pitch, which varies from $-\pi$ to $\pi$. Consider, for instance, a particular value of the constant of integration, say, $C_i < 1$ and the curve $\zeta_i = \zeta\ (\psi,C_i)$, which pertains to that constant. Assume that at the moment of time $t_0$ a larva has initial coordinates $(\zeta_0, \psi_0)$ which correspond to a certain point of the curve. For anther moment of time $t_1 > t_0$ the angle of turn $\psi$ grows and another pair of coordinates $(\zeta_1, \psi_1)$ gives another point of the same curve. If we continue this process, all such points will draw a curve which corresponds to the constant $C_i$. This process of drawing the curve by a moving point is indicated in Fig. 22 by arrows.

The point of intersection of a curve of the diagram with a boundary (boundaries) determines the coordinates of the particle in the moment of contact. For any curve crossing a bounding line any of its points $(\zeta_0, \psi_0)$ can be considered as an initial one. Then, a larva-particle starting the motion with this initial condition will eventually reach the boundary (boundaries).

The coordinate of the intersection point of the curve $\zeta = \zeta\ (\psi,\ C)$ with the boundaries are $\zeta = 0$ or $\zeta = 1$. We are interested neither in these coordinates, nor in the moment of time when contact takes place, but in the fact of crossing of the boundary (boundaries) by curves $\zeta = \zeta(\psi,C)$, i.e., in the fact of contact.

The further analysis is carried out, by using the diagram in Fig. 22 for two separate cases, $\lambda > 2$ (Fig. 22a) and $\lambda \leq 2$ (Fig. 22b), correspondingly. In Fig. 22 the line $\zeta(\psi,\ C = 1)$ (separatrix) divides the domain $(0 < \zeta < 1,\ -\pi < \psi < \pi)$ into two subdomains. All curves which are located below the separatrix correspond to constants $C < 1$. All curves which

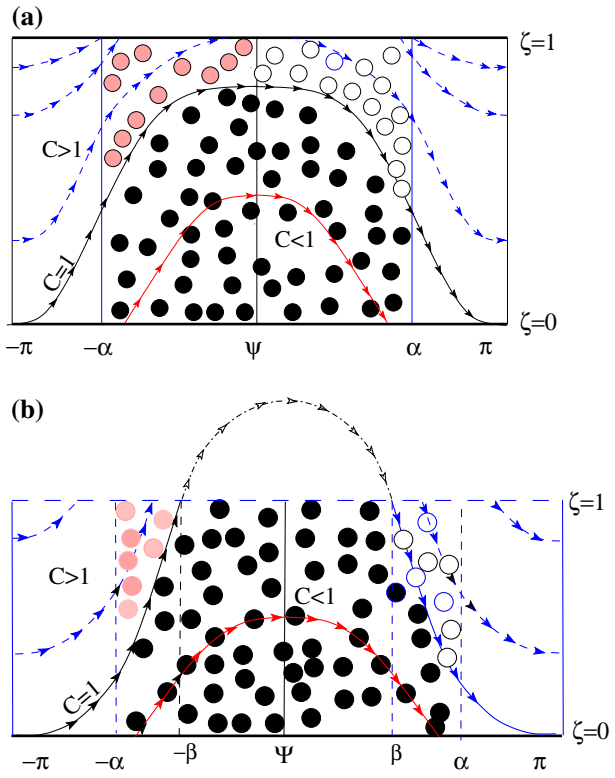


**Fig. 22** Linear shear flow: the coordinate of a particle $\zeta$ as function of its angle of turn $\psi$. **a** $-\lambda = U_d/V_S > 2$; **b** $-\lambda \leq 2$. The line $\zeta = 0$ represents the non-dimensional coordinate a fixed wall; the line $\zeta = 1$ represents another wall, which moves with a given velocity (Couette flow) or the upper bound of the linear boundary layer. The line which corresponds to the constant of integration $C$ touches the boundary $\zeta = 0$ and separates the domain $0 < \zeta < 1$ into two subdomains which contain curves corresponding to constants of integration $C < 1$ or $C > 1$. In the Couette flow bounded by two wall curves $\zeta = \zeta(\psi,C)$ may cross the lower wall (*black circles*), the upper wall (*gray circles*) or none of them (*white circles*). In the linear boundary, layer the curves $\zeta = \zeta(\psi,C)$ with *black points* may cross the lower boundary; whereas the *white* and *gray* particles do not

are located above the separatrix correspond to constants $C > 1$. All curves corresponding to $C < 1$ cross the lower boundary. Any point which belong to the area bounded by the curve $\zeta(\psi,C = 1)$ and line $\zeta = 0$ crosses the boundary because it belongs to a certain curve $\zeta(\psi,C < 1)$. All such points are depicted as black circles. Points which are depicted as white circles belong to the domain $C > 1$; they do not cross the boundary $\zeta = 0$. If the line $\zeta = 1$ represents the wall of the Couette channel, the gray points should be counted as those, which contact the upper wall. However, if the line $\zeta = 1$ represents the boundary of the linear boundary layer the gray points should be counted as those, which do not contact the boundary.

For the further calculations it is assumed that larvae are distributed randomly and uniformly within the range (0, 1) and that the initial angles of turn are also random numbers distributed uniformly in the range $(-\alpha, \alpha)$, where $\alpha \leq \pi$.

If we take a sufficiently large number of points (an infinite in a limiting case) they will fill corresponding areas. The area, which is filled by particles, crossing the boundary (boundaries) divided by the area filled by all particles can be defined as the probability of contact. It is not difficult to calculate the contact probability for all possible cases, considered above. However, for the sake of brevity we give here formulas for contact probability only for the linear boundary layer.

For $\lambda > 2$ (Fig. 22a) the probability of contact $P$ can be approximated as the ratio of the area filled by black points and the total area $S_0 = 2\alpha$. Simple calculations of the corresponding areas yield the contact probability in the following form:

$$P = \frac{1}{\lambda}\left(1 + \frac{\sin\alpha}{\alpha}\right). \tag{I.2}$$

For $\lambda < 2$ the calculations of the contact probability are somewhat more complicated because it is necessary to take into account the fact that the line $\zeta = 1$ crosses the curve $\zeta(\psi,C = 1)$ at the points $\beta = 2\arcsin\sqrt{1 - \lambda/2}$ (Fig. 22b) and the result depends on the sign of the difference $\alpha - \beta$. Similarly to the previous case, the contact probability can be calculated as the ratio of two areas, one with black points and the other one including all particles. A closer scrutiny of Fig. 22b and simple calculations of the corresponding areas give the contact probability in the following form:

$$P = \begin{cases} 1 & \beta \geq \alpha, \\ \frac{1}{\alpha}\left[\beta + \frac{1}{\lambda}(\alpha - \beta + \sin\alpha - \sin\beta)\right] & \beta < \alpha. \end{cases} \tag{I.3}$$

If we assume that all larvae enter the vortical flow with the same zero initial angle of turn ($\alpha \to 0$) then formulae I.2 and I.3 can be greatly simplified, yielding Eq. 51. Expressions I.2–I.3 are plotted in Fig. 16.

## Appendix II

In this Appendix, we derive a closed form solution for the probability of contact of larvae moving in a plane Poiseuille channel. It many details the corresponding analysis is similar to that given in Appendix I for a linear shear flow. Therefore, for the sake of brevity, we give here only the principal details of the calculations.

Introduce first the non-dimensional variables $\xi = X_O/R$, $\zeta = Z_O/R$ and $\tau = U_a\, t/R$. In non-dimensional coordinates the boundaries of the channel are represented by lines $\zeta = \pm 1$. It is assumed that the initial coordinates of larvae $\zeta_0$ and the initial angles of turn $\psi_0$ are represented by random numbers which are distributed uniformly in the rectangle $|\zeta_0| < 1$ and $|\psi_0| < \alpha \leq \pi$.

Although the analytic solution of Eqs. 39–41 is unknown, the contact probability can still be expressed in a closed form.

For the case of a neutrally buoyant larva Eqs. 39–41 can be easily reduced to the differential equation of a pendulum

$$\frac{d^2\psi}{d\tau^2} = 2\frac{\sin\psi}{\lambda}, \tag{II.1}$$

which can be transformed into a so-called phase portrait of a pendulum

$$\frac{d\psi}{d\tau} = \pm 2\sqrt{\frac{C-\cos\psi}{\lambda}}. \tag{II.2}$$

Here $C$ is a constant of integration, which is determined by the angle of turn and its derivative with respect to non-dimensional time (Jordan and Smith 1987). Using Eq. 41 the phase portrait can be transformed into a parametric dependence, which is more convenient for our purposes:

$$\zeta(\psi, C) = \pm\sqrt{\frac{C-\cos\psi}{\lambda}}, \tag{II.3}$$

where the constant of integration is now determined by a pair of numbers ($\zeta_0$, $\psi_0$). Relation Eq. II.3 is plotted in Fig. 23 and represents closed and open curves with a separatrix $\zeta(\psi, C = 1)$. Denoting the curve which touches the wall $\zeta = \pm 1$ at the points $\psi = \pm\pi$ as $\zeta_l(\psi) = \pm\zeta(\psi, C_l)$, the value of the corresponding constant of integration $C_l$ can be obtained as a solution of an algebraic equation $\pm\zeta(\pm\pi, C_l) = \pm 1$ yielding $C_l = \lambda - 1$ and

$$\zeta_l(\psi) = \pm\sqrt{\frac{\lambda-1-\cos\psi}{\lambda}}. \tag{II.4}$$

Analysis of Fig. 23a shows that for $\lambda > 2$ the probability of contact can be calculated as the ratio of the area with black points and the total area filled by all points. Calculating the ratio of the two areas yields

$$P = 1 - \frac{1}{\alpha}\int_0^{\alpha}\sqrt{\frac{\lambda-1-\cos\psi}{\lambda}}d\psi. \tag{II.5}$$

For $\lambda \le 2$, the limiting curves $\zeta_l$ cross the axis $\zeta = 0$ at angles $\beta = \pm\arccos(\lambda - 1)$ (Fig. 23b). In Fig. 23b, we have three types of points. The white particles belong to closed curves which do not cross the boundary. Once again, the probability of initial contact can be calculated as the ratio of the area with black and gray points and the total area of the corresponding rectangle $2\alpha$, which includes all symbols. Analytic calculations of the corresponding areas show that for $\lambda \le 2$ the probability of initial contact is given by

$$P = \begin{cases} 1, & \beta \ge \alpha, \\ 1 - \frac{1}{\alpha}\int_{\beta}^{\alpha}\sqrt{\frac{\lambda-1-\cos\psi}{\lambda}}d\psi, & \beta < \alpha. \end{cases} \tag{II.6}$$

If we assume that all larvae enter the vortical flow with the same zero initial angle of turn ($\alpha \to 0$) formulae (II.5) and II.6 become very simple yielding 52.

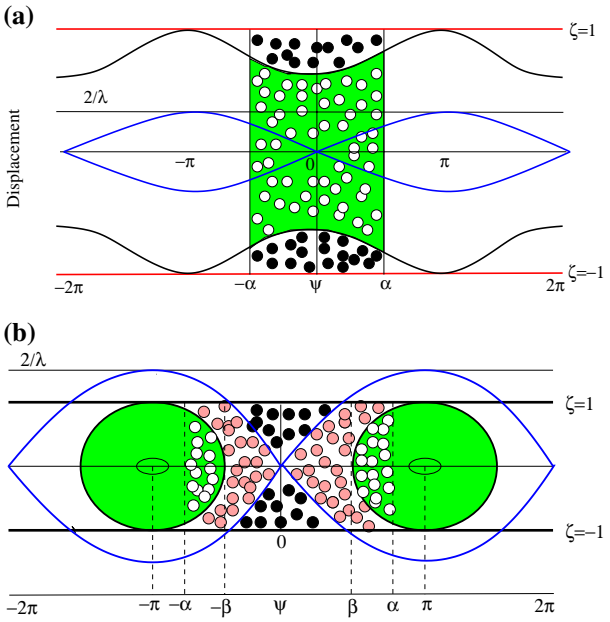


**Fig. 23** Plane Poiseuille flow: the coordinate of a particle $\zeta$ as function of its angle of turn $\psi$. **a** $\lambda > 2$, **b** $\lambda \le 2$. The walls of the channel are represented by lines $\zeta = \pm 1$. The range of the possible initial angles of larvae turns is denoted as $(-\alpha,\alpha)$. The diagram consists of closed and unclosed curves divided by a separatrix. In (**a**) are plotted the bounds of the channel, two symmetric unclosed curves, touching the boundary, and the separatrix; whereas the closed curves, which are encircled by the separatrix are not shown. The separatrix does not cross the bounds and only curves that are formed by black point (black circles) cross the rigid boundaries. The white particles on a gray background belong to curves, which do not cross the bounds. A large number of white and black particles cover certain areas. The ratio of the area filled by white particles and the total area filled by all particles is defined as the probability of contact. In (**b**) the separatrix crosses or touches the lines $\zeta = \pm 1$. Therefore, both types of curves, closed and unclosed may cross the boundary. The coordinate of intersection of the separatrix and the bounding lines is denoted as $|\beta| = \arccos(\lambda - 1)$. For the initial angles of pich $|\psi_0| < \alpha$ and $|\beta| \ge \alpha$ open curves, which are formed by black points, and closed curves, which are formed by gray, circles cross the boundary. Closed curves, which are formed by white circles on a gray background do not cross the boundaries. The probability of contact is the ratio of the area filled by black and gray particles and the total area filled by all particles. If $|\beta| < \alpha$ (the case which is not shown on the diagram) only black and gray points has to be taken into account. Since black and gray particles form curves, which always cross the bounds the probability of contact is equal to one

Relations II.5 and II.6 incorporate integrals, which are computed here numerically with a relative error of less than 0.1%. The results of computations for different values of the parameters involved are plotted in Fig. 16.

## Appendix III

The coordinates of $N$ particles randomly and uniformly distributed inside a circle of radius $R$ are calculated as follows (Sobol 1994):

$$X_{Oi} = R\sqrt{\gamma_{1i}}\cos 2\pi\gamma_{2i} \text{ and } Z_{Oi} = R\sqrt{\gamma_{1i}}\sin 2\pi\gamma_{2i} \quad (i = 1, 2, \cdots N), \qquad \text{(III.1)}$$

where $\gamma_{1,2}$ are distinct random numbers distributed uniformly between 0 and 1. We also assume that the initial direction of the self-propulsion vector is represented by random angles distributed uniformly in the range $(-\alpha, \alpha)$ as $\sigma = (2\gamma_\sigma - 1)\alpha$, where $\sigma$ is one of the Euler angles $|\alpha| < \pi$ and $\gamma_\sigma$ is a random number distributed uniformly between zero and one.

## Appendix IV

In the right-hand orthogonal coordinate system $O_1XYZ$ with vector units of the axes $\mathbf{j}_X$, $\mathbf{j}_y$ and $\mathbf{j}_Z$ correspondingly, the mathematical operation curl $\mathbf{U}$ is given by a determinant

$$\begin{aligned}\operatorname{curl}\mathbf{U} &\equiv \begin{vmatrix} \mathbf{j}_X & \mathbf{j}_Y & \mathbf{j}_Z \\ \frac{\partial}{\partial X} & \frac{\partial}{\partial Y} & \frac{\partial}{\partial Z} \\ U_X & U_Y & U_Z \end{vmatrix} \\ &= \mathbf{j}_X\left(\frac{\partial U_Z}{\partial Y} - \frac{\partial U_Y}{\partial Z}\right) - \mathbf{j}_Y\left(\frac{\partial U_Z}{\partial X} - \frac{\partial U_X}{\partial Z}\right) \\ &\quad + \mathbf{j}_Z\left(\frac{\partial U_Y}{\partial X} - \frac{\partial U_X}{\partial Y}\right).\end{aligned}$$

In the case of a two-dimensional motion when the fluid velocity vector is located in the plain $O_1XZ$, the vector of the vorticity has only one component

$$\operatorname{curl}_2\mathbf{U} = \left(\frac{\partial U_X}{\partial Z} - \frac{\partial U_Z}{\partial X}\right)\mathbf{j}_Y,$$

which is directed perpendicularly to the plane $O_1XZ$. In the case of a linear shear flow when the vector of fluid velocity is parallel to the axis $O_1X$ and depends linearly on the coordinate $Z$ the vorticity vector is equal to the constant gradient of the fluid velocity. In this particular case the absolute value of the vorticity vector and of the value of the rate of shear are expressed by the same gradient of the velocity in the direction perpendicular to its vector, i.e., by $\partial U_X/\partial Z$.

## References


Abelson A, Denny M (1997) Settlement of marine organisms in flow. Ann Rev Ecol Syst 28:317–339

Abelson A, Miloh T, Loya Y (1993) Flow patterns induced by substratum and body morphology of benthic organisms, and their role in determining food particle availability. Limnol Oceanogr 38:1116–1124

Abelson A, Weihs D, Loya Y (1994) Hydrodynamic impediments to settlement of marine propagules, and adhesive-filament solutions. Limnol Oceanogr 39:164–169

Achenbach E (1968) Distribution of local pressure and skin friction around a circular cylinder in cross-flow up to Re = 5 × $10^6$. J Fluid Mech 34:625–639

Archer D, Emerson S, Smith CR (1989) Direct measurement of the diffusive sublayer at the deep sea floor using oxygen microelectrodes. Nature 340:623–626

Butman A, Grassle JP, Webb CM (1988) Substrate choices made by marine larva settling in still water and in a flume flow. Nature 333:771–773

Caldwell DR, Chriss TM (1979) The viscous sublayer at the sea floor. Science 205:1131–1132

Crimaldi JP, Thompson JK, Rosman JH, Lowe RJ, Koseff JR (2002) Hydrodynamics of larval settlement: the influence of turbulent stress events at potential recruitment sites. Limnol Oceanogr 47:1137–1151

Crisp DJ (1955) The behavior of barnacle cyprids in relation to water movement over a surface. J Exp Biol 32:569–590

Denny MW, Shibata MF (1989) Consequences of surf-zone turbulence for settlement and external fertilization. Am Nat 134:859–889

Denny MW, Nelson EK, Mead KS (2002) Revised estimates of the effects of turbulence on fertilization in the Purple Sea Urchin, *Strongylocentrotus purpuratus*. Biol Bull 203:275–277

Eckman JE (1990) A model of passive settlement by planktonic larvae onto bottom of different roughness. Limnol Oceanogr 35:887–901

Eckmann JE (1996) Closing the larval loop: linking larval ecology to the population dynamics of marine benthic invertebrates. J Exp Mar Biol Ecol 200:207–237

Eckman JE, Duggins DO (1998) Larval settlement in turbulent pipe flows. J Mar Res 56:1285–1312

Fredsøe J, Deigaard R (1992) Mechanics of coastal sediment transport. World Scientific, Singapore

Fuchs NA (1964) The mechanics of aerosols. Pergamon Press, Oxford

Goldstein H, Poole C, Safko J (2002) Classical mechanics. Addison Wesley, New York

Grünbaum D, Strathnman RR (2003). Form, performance and trade-offs in swimming and stability of armed larvae. J Mar Res 61:659–691

Happel J, Brenner H (1983) Low Reynolds number hydrodynamics with special application to particulate media. Noordhoff, Leyden

Hart D, Finlelli CM (1999) Physical-biological coupling in stream: the pervasive effects of flow on benthic organisms. Annu Rev Ecol Syst 30:363–395

Jeffrey GB (1922) The motion of ellipsoidal particles immersed in a viscous fluid. Proc R Soc Lond 102:161–169

Jonsson PR (2005) A classical hydrodynamic analysis of larval settlement. Exp Biol 208:3431–3432

Jonsson PR, Andre C, Lindegarth M (1991) Swimming behavior of marine bivalve larvae in a flume boundary-layer flow: evidence for near-bottom confinement. Mar Ecol Prog Ser 79:67–76

Jonsson PP, Berntsson KM, Larsson AI (2004) Linking of larval supply to recruitment: flow mediated control of initial adhesion of barnacle larvae. Ecology 85:2850–2858

Jordan DW, Smith P (1987) Nonlinear ordinary differential equations. Oxford University Press, Oxford

Karp-Boss L, Boss E (2000) Motion of dinoflagellates in a simple shear flow. Limnol Oceanogr 45:1594–1602

Karp-Boss L, Jumars PA (1998) Motion of diatom chains in a steady shear flow. Limnol Oceanogr 43:1767–1773

Kessler JO (1986) The external dynamics of swimming micro-organisms. In: Round FE, Chapman DJ (eds) Progess in phycological research 4. Biopress, Bristol, pp. 258–307

Lamb H (1945) Hydrodynamics, 6th edn. Dover, New York

Larsson AI, Jonsson PR (2006) Barnacle larvae actively select flow environments supporting post-setlment growth and survival. Ecology 87:1960–1966

Lynch WF (1947) The behavior and metamorphosis of the larva of Bugula Neritina (linnaeus): experimental modification of the

length of the free-swimming period and the responses of the larvae to light and gravity. Biol Bull 92:115–150
Maldonado M (2006) The elocogy of the sponge larva. Can J Zool 84:175–194
Mullinaux LS, Butman CA (1991) Initial contact, exploration and attachment of barnacle (*Balanus amphitrite*) cyprids settling in the flow. Mar Biol 110:93–103
Mullineaux LS, Garland ED (1993) Larval recruitment in response to manipulated field flows. Mar Biol 116:667–683
Mullineax LS, Butman CA (1990) Recruitment of benthic encrusting invertebrates in boundary-layer flow: a deepwater experiment on Cross Seamount. Limnol Oceanogr 35:409–423
Nilsen P (1992) Coastal bottom boundary layer and sediment transport. World Scientific, Signapore
Pasternak Z, Blasius B, Abelson A (2004) Host location by larvae of a parasitic barnacle: larval chemotaxis and plume tracking in flow. J Plankt Res 26:487–493
Pedley TJ, Kessler JO (1992) Hydrodynamic phenomena in suspension of swimming microorganisms. Annu Rev Fluid Mech 24:313–358
Perkol-Finkel S, Zilman G, Sella I, Miloh T, Benayahu Y (2006) Floating and fixed artificial reefs: the effect of substratum on motion on benthic communities in a coral reef environment. Mar Ecol Prog Ser 317:9–20
Pires A, Woollacott RM (1983) A direct and active influence of gravity on the behavior of marine invertebrate larva. Science 220:731–733
Qian PY, Rittschof D, Sreedhar B, Chia F (1999) Macrofouling in unidirectional flow: miniature pipes as experimental models for studying the effects of hydrodynamics on invertebrate larval settlement. Mar Ecol Prog Ser 191:301–303
Qian PY, Rittschof D, Sreedhar B (2000) Macrofouling in unidirectional flow: miniature pipes as experimental models for studying the interaction of flow and surface characteristics on the attachment of barnacle, bryozoan and polichaete larvae. Mar Ecol Prog Ser 207:109–121
Roshko A (1961) Experiments on the flow past a circular cylinder at very high Reynolds number. J Fluid Mech 10:345–356
Schlichting H (1979) Boundary layer theory, 7th edn. McGraw Hill Co, New York
Scorer RS (1978) Environmental aerodynamics. Wiley, London
Segre G, Silberberg A (1962) Behavior of macroscopic rigid spheres in Poiseuille flow, Part II. Experimental results and interpretation. J Fluid Mech 14:136–157
Seinfeld JH, Pandis SN (1998) Atmospheric chemistry and physics. From air pollution to climate change. Wiley, New York
Sobol IH (1994) A premier for the Monte Carlo method. CRC Press, Boca Raton
Sugihara-Seki M (1996) The motion of an ellipsoid in tube flow at low Reynolds numbers. J Fluid Mech 324:287–308
Swaminathan TN, Mukuundakrishnan K, Hu HH (2006) Sedimentation of an ellipsoid inside an infinitely long tube at low and intermediate Reynolds numbers. J Fluid Mech 551:357–385
Walters LJ, Hadfield MG, Carmen KA (1997) The importance of larval choice and hydrodynamics in creating aggregations of *Hydroides elegans* (Polycheta: Serpulidae). Invertebr Biol 116:102–114
Walton Smith FG (1946) Effect of water current upon the attachment and growth of barnacles. Biol Bull Woods Hole 90:51–70
Wendt DE (2000) Energetics of larval swimming and metamorphosis in four species of *Bugula* (Bryozoa). Biol Bull 198:346–356